GGA2 and RAB13 regulate activity-dependent β1-integrin recycling

Pranshu Sahgal[1], Jonna Alanko[1,#], Ilkka Paatero[1], Antti Arjonen[1,$], Mika Pietilä[1], Anne Rokka[1], Johanna Ivaska[1,2,*]

[1]Turku Centre for Biotechnology, University of Turku and Åbo Akademi University, Turku FIN-20520, Finland

[2]Department of Biochemistry and Food Chemistry, University of Turku, Turku FIN- 20520, Finland

[#] Current address: IST Austria, Klosterneuburg 3400, Austria

[$] Current address: Misvik Biology, Turku FIN-20520, Finland

* corresponding author: joivaska@utu.fi

Abstract

β1-integrins mediate cell-matrix interactions and their trafficking is important in the dynamic regulation of cell adhesion, migration and malignant processes like cancer cell invasion. Here we employ unbiased RNAi screening to characterize regulators of integrin traffic and identify the association of Golgi-localized gamma ear-containing Arf-binding protein 2 (GGA2) with β1-integrin and its role in recycling of the active but not inactive β1-integrins. Silencing of GGA2 limits active β1-integrin levels in focal adhesions and decreases cancer cell migration and invasion congruent with its ability to regulate the dynamics of active integrins. Using the proximity-dependent biotin identification (BioID) method, we identify two RAB family small GTPases, RAB13 and RAB10, associating with GGA2 and β1-integrin. Functionally, RAB13 silencing triggers the intracellular accumulation of active β1-integrin, identically to GGA2 depletion, indicating that both facilitate recycling of active β1-integrins to the plasma membrane. Thus, GGA2 and RAB13 are important specificity determinants for integrin activity-dependent traffic.

Introduction

Cancer cell migration is a complicated process involving the spatiotemporal control of cell adhesion dynamics on multiple levels. Integrins are the main adhesion receptors for extra-cellular matrix (ECM) ligands. They consist of 18 α- and 8 β-subunits and can form 24 heterodimers for different extracellular matrix ligands (Hynes 2002, Kawauchi 2012). Integrin-

mediated cell-ECM interactions are influenced by integrin expression levels, regulation of integrin activity (i.e., their affinity for ECM ligands) and their endo/exosomal trafficking on the plasma membrane. Integrin activity in adherent cell types, like carcinoma cells and fibroblasts, is most likely defined by a continuum of receptor conformations where the fully inactive bent receptor switches in response to integrin activating proteins, such as talin and kindlin, into the fully active extended and ligand-bound receptor (Ye, Snider et al. 2014, Calderwood, Campbell et al. 2013a). Deregulated integrin activity is implicated in multiple pathological conditions (Winograd-Katz, Fassler et al. 2014, Pozzi, Zent 2013, Hegde, Raghavan 2013). In cancer cells, increased integrin activity, triggered either by increased expression of integrin activating proteins (Calderwood, Campbell et al. 2013b) or reduced expression of inactivating proteins (Liu, Das et al. 2015, Rantala, Pouwels et al. 2011), has been linked to increased migration and invasion (Jin, Tien et al. 2015, Felding-Habermann, O'Toole et al. 2001).

Integrins undergo constant endo/exocytosis from the cell membrane and this is important to provide directionality to the cell and assists in the formation and release of cell-substrate contacts for proper cell movement (Kawauchi 2012, Fletcher, Rappoport 2010). Thus, the balance between internalized and cell-surface integrins within cells plays a critical role in cell migration. Altered integrin trafficking, especially in the case of β1-integrins, is linked to invasive processes (Bridgewater, Norman et al. 2012, De Franceschi, Hamidi et al. 2015, Parachoniak, Park 2012). Furthermore, recent studies have reported the presence of active integrins inside endosomes (Alanko, Mai et al. 2015, Rainero, Norman 2015) and a link between directed integrin traffic, from talin and FAK-positive endosomes to the plasma membrane, to the reassembly of focal adhesions at the leading edge of migrating cells (Nader, Ezratty et al. 2016). Previous work, from us, has shown that the net endocytosis rate of active β1-integrins is higher than inactive β1-integrins (Arjonen, Alanko et al. 2012). Active β1-integrins recycle predominantly through RAB11-dependent long-loop pathways whereas inactive β1-integrins recycle through RAB4 and actin-dependent short-loop recycling pathways or undergo retrograde traffic through the trans-Golgi network (Powelka, Sun et al. 2004a, Arjonen, Alanko et al. 2012, Campbell, Humphries 2011). However, apart from some, more specific conditions such as RAB25- and CLIC3-expressing carcinomas (Dozynkiewicz, Jamieson et al. 2012), the mechanistic details of the trafficking pathways that differentially regulate integrin dynamics based on receptor activity remain poorly understood. Furthermore,

very little is known about how different endosomal adaptor proteins contribute to integrin traffic and cell migration.

The GGA (Golgi-localized gamma ear-containing Arf-binding protein) family of adaptors (GGA1, GGA2, GGA3) was first described in the year 2000 and originally identified as Arf effectors, interacting with clathrin-coated vesicles and localizing to the trans-Golgi network and endosomes (Boman, Zhang et al. 2000, Dell'Angelica, Puertollano et al. 2000, Puertollano, Randazzo et al. 2001, Puertollano, Bonifacino 2004). Even though the mammalian GGAs are thought to be at least partially redundant (Hirst, Lui et al. 2000, Dell'Angelica, Puertollano et al. 2000, Govero, Doray et al. 2012), several studies have indicated specific non-overlapping and even opposite functions for GGA-family members. In mice, genetic deletion of GGA1 or GGA3 alone is well tolerated whereas the loss of GGA2 results in embryonic or neonatal lethality (Govero, Doray et al. 2012), indicating important specific biological functions for GGA2. Moreover, GGA1 and GGA3, but not GGA2, recognize ubiquitin (Puertollano, Bonifacino 2004, Scott, Bilodeau et al. 2004, Shiba, Katoh et al. 2004) and have been implicated in the degradation of endocytosed EGFR. While GGA3 or GGA1 depletion promotes EGFR expression, GGA2 depletion, in contrast, drastically reduces EGFR levels through an unknown mechanism (Uemura, Kametaka et al. 2018). In addition, GGA1 and GGA3 are specifically required for endosomal recycling of transferrin (GGA1) and MET receptor tyrosine kinase (GGA3) and in facilitating stability of collagen-binding integrin α2β1 (GGA3) by diverting it away from lysosomal degradation (Zhao, Keen 2008a, Parachoniak, Luo et al. 2011, Ratcliffe, Sahgal et al. 2016). In contrast, GGA2 has not been implicated in integrin traffic.

Here we have investigated the role of the GGA adaptor family in regulating β1-integrin traffic in breast cancer cells and identify a previously undescribed role for GGA2 in driving recycling of active β1-integrins and regulating cell motility and invasion.

Results

GGA2 regulates β1-integrin traffic

The coordinated traffic of integrins through the endolysosomal network must be tightly regulated to enable efficient cell motility. Unlike many other cell-surface receptors, integrins have a remarkably long half-life suggesting that following endocytosis the majority of integrins

are efficiently recycled back to the plasma membrane. We recently identified a critical role for GGA3 in diverting the collagen receptor α2β1 integrin away from lysosomal degradation to support HeLa cell migration on collagen (Ratcliffe, Sahgal et al. 2016). This prompted us to investigate whether other GGAs or their known interactors (based on BioGrid server) regulate integrin traffic. We conducted a β1-integrin endocytosis screen employing a quenching-based β1-integrin antibody endocytosis assay (Arjonen, Alanko et al. 2012) adapted to the cell spot microarray RNAi screening platform (Rantala, Makela et al. 2011). Focusing on GGAs and their interactors, we consistently observed a significant increase in intracellular β1-integrin levels, after 30 minutes of endocytosis, upon GGA2 silencing with two independent siRNAs in MDA-MB-231 cells (Fig. S1A). To confirm the role of GGA2 in β1-integrin dynamics, we performed biotin-IP-based β1-integrin endocytosis assays in GGA2-silenced (GGA2 siRNA#1 is distinct from the RNAi oligos used in the screen) MDA-MB-231 cells. In line with the RNAi screen, depletion of GGA2 with significantly increased the level of intracellular β1-integrin at 10 and 20 minute time points without influencing total β1-integrin expression levels (Fig. 1A,B; S1B). Conversely, overexpression of GGA2 significantly reduced β1-integrin uptake (Fig. 1C,D). In contrast to GGA1 depletion (Zhao, Keen 2008b), silencing of GGA2 did not influence internalization of the transferrin receptor, suggesting a specific role for GGA2 in integrin receptor traffic (Fig. S1C,D).

GGA2 regulates specifically the dynamics of active β1-integrins

Many studies have indicated that β1-integrins recycle to the plasma membrane with a turnover rate of 10-15 minutes (Argenzio, Margadant et al. 2014, Diggins, Kang et al. 2018, Dozynkiewicz, Jamieson et al. 2012). The slow accumulation of β1-integrin inside GGA2-silenced cells led us to hypothesise that receptor recycling, rather than endocytosis, is affected by the loss of GGA2 expression. Indeed, the recycling inhibitor primaquine fully abolished the observed trafficking difference between control- and GGA2-silenced cells (Fig. 1E,F), indicating that GGA2 silencing increases intracellular β1-integrin levels by inhibiting recycling rather than stimulating endocytosis.

To confirm the specificity of these findings and the implications for active and inactive pools of β1-integrins, we silenced GGA2 with a fourth independent siRNA (GGA2 siRNA#2 is distinct from the RNAi oligos used in the screen) and analysed the levels of cell-surface labelled active and inactive β1-integrins, following internalisation, using flow cytometry (Fig. 1G,H). Interestingly, GGA2 silencing specifically reduced the cell-surface levels of active, but

not inactive β1-integrin, in comparison to control silenced cells, following 15 and 30 minutes of endocytosis (Fig. 1G,H), suggesting selective intracellular accumulation of the active receptor in the absence of GGA2. Further immunofluorescence analyses of control- and GGA2-silenced cells plated on micropatterns (Thery 2010) supported the results obtained with the biotin- and flow cytometry-based integrin trafficking assays, and demonstrated a significant increase in the steady-state pool of intracellular active β1-integrin upon GGA2 silencing (Fig. 1I,J).

We have previously shown that active and inactive integrins return to the plasma membrane with different kinetics (Arjonen, Alanko et al. 2012). However, to date, the molecules regulating traffic of these distinct integrin pools have remained enigmatic. Therefore, we were interested to study further the requirement for GGA2 in regulating traffic of active β1-integrin in cells. Immunofluorescence imaging of cell-surface-labelled active β1-integrin, following different times of internalization, revealed a significant increase in the intracellular accumulation of active β1-integrin in endosome-like structures in GGA2-silenced cells (Fig. 2 A,B). These puncta were significantly reduced by overexpression of GFP-GGA2 (Fig. 2 C,D) and the partial overlap was detected between the internalized active-β1 and GFP-GGA2 (Fig. 2C). In contrast, GFP-GGA2 expression had no significant effect in internalization of cell-surface-labelled inactive-β1 integrin (Fig. S2A, B). Inhibition of receptor recycling with primaquine abolished the difference in active β1-integrin internalization between GFP and GFP-GGA2 expressing cells (Fig. 2E,F), further validating a role for recycling in GGA2-regulated integrin traffic in these cells. Interestingly, GFP-pulldowns of GFP-GGA2, but not GFP alone, co-precipitated endogenous β1-integrin (Fig. 2G), suggesting that the ability of GGA2 to direct β1-integrin trafficking may be linked to their association in cells.

GGA2 localises to endosomes and the plasma membrane

GGA2 has been studied predominantly in yeast and its subcellular localization in cancer cells is less well characterized. We performed immunofluorescence staining of endogenous GGA2 and endogenous markers for different endomembrane compartments. GGA2 overlapped with early endosomal marker RAB5 and with recycling endosomes positive for RAB4 or RAB11 (Fig. 3A). In addition, partial overlap was detected with early endosomal marker EEA1 and with VPS35, a component of the retromer complex (Fig. 3A). GGA2 did not colocalise with late endosome/lysosome markers RAB7 and LAMP1 (LAMP1 was stained in GFP-GGA2-expressing cells, as antibodies against LAMP1 and endogenous GGA2 are raised in the same

species). Thus, in MDA-MB-231 cells, GGA2 localises to early and recycling endosomes in addition to its established localization to TGN46 labelled trans-Golgi network, RAB6-positive Golgi vesicles and clathrin-coated vesicles (Fig. S3A) (Zhu, Doray et al. 2001a, Hirst, Lui et al. 2000). Next, we analysed further the subcellular localization of GGA2 and β1-integrin. GGA2 colocalised with β1-integrin in intracellular vesicles (β1-integrin was stained in GFP-GGA2-expressing cells, as antibodies against β1-integrin and endogenous GGA2 are raised in the same species) (Fig. 3B). Interestingly, GGA2 was detected on the plasma membrane in regions positive for active β1-integrin (Fig. 3C). This original observation of GGA2 plasma membrane staining was further validated using total internal reflection microscopy (TIRF) that enables visualization within 200 nm of the plasma membrane (Fig. S3B). Consistently, biochemical fractionations separating plasma membrane and cytoplasmic proteins (Bass, Williamson et al. 2011a) demonstrated the presence of GGA2 in the β1-integrin-positive plasma membrane fraction (Fig. S3C,D). Together, these results demonstrate that GGA2 associates with β1-integrin and localises to early and recycling endosomes as well as to the plasma membrane, and facilitates active β1-integrin recycling to the cell surface.

GGA2 regulates focal adhesions, cell migration and cancer cell invasion

β1-integrins are the main receptors for extracellular matrix proteins (Jean, Gravelle et al. 2011, Huang, Rofstad 2018) and their endo/exocytic trafficking is a key regulator of cell-ECM interactions and cell motility. To investigate whether GGA2 regulates focal adhesions, we plated control- and GGA2-silenced cells on a mixture of collagen and fibronectin and analysed the number and size of paxillin-positive focal adhesions. GGA2 silencing had no significant effect on focal adhesion number (Fig. 4A) but significantly reduced the levels of active β1-integrin in the adhesions 30 minutes after plating and the lower active β1-integrin levels were maintained up to 2 hours post plating (Fig. 4B). Recycling of β1-integrins is essential for cell migration speed and for effective cancer cell invasion (Paul, Allen et al. 2015, Caswell, Chan et al. 2008). Most pathways described thus far are not specific to integrin activity status (Paul, Jacquemet et al. 2015) and hence we were interested to determine how inhibition of active β1-integrin recycling influences cancer cell motility and invasion. Time-lapse microscopy of MDA-MB-231 cells migrating on collagen revealed that GGA2-silenced cells display significantly slower migration speeds, with no difference in persistence (Fig. 4C, Fig. S4A). Furthermore, GGA2 depletion reduced cancer cell invasion in three-dimensional collagen (Fig. 4D) and in zebrafish embryo xenografts (Fig. 4E). These effects were specifically due to reduced cell motility and altered adhesions since GGA2 silencing did not influence cell

proliferation in 2D or in suspension or the size of zebrafish embryo xenografts (Fig. S4B,C, D). Together, these results show that interfering with the GGA2-dependent delivery of active β1-integrins to the plasma membrane leads to defective focal adhesion formation, reduced cell motility and impaired cancer cell invasion in vitro and in vivo.

Proximity biotinylation identifies new GGA2-associated trafficking proteins

All GGA-family members share the VHS domain, which binds cargo proteins with a cytosolic acidic di-leucine (AC-LL) motif, and regulate trafficking of e.g. mannose-6-phosphate receptor and sortilin via this mechanism (Takatsu, Katoh et al. 2001, Nielsen, Madsen et al. 2001). β1-integrins lack this motif, suggesting that alternative mechanisms are involved in the GGA2-dependent traffic of active β1-integrins. To investigate this further, we employed in-situ labelling of GGA2-proximal components in intact cells by fusing GGA2 with BirA (BioID) and myc-tag to enable visualization of the protein (Roux, Kim et al. 2012). Importantly, myc-BioID-GGA2 localised similarly to GFP-GGA2 to a perinuclear compartment (Golgi), a pool of endosomes and the plasma membrane and efficiently catalysed in situ biotinylation of these compartments in biotin-treated cells (Fig. S5B). In contrast, myc-BioID alone did not overlap with GFP-GGA2 in cells and displayed uniform, non-compartmentalized biotinylation of the cytosol (Fig. S5B). The specificity and efficiency of this approach was further validated by isolating biotinylated proteins from myc-BioID- or myc-BioID-GGA2-expressing cells. Known GGA2 interacting proteins including clathrin, GGA1 and GGA3 (Zhu, Doray et al. 2001b, Ghosh, Griffith et al. 2003) were detected in streptavidin pulldowns only in myc-BioID-GGA2-expressing cells, indicating functionality and specificity of the in situ biotinylation approach (Fig. S5C).

To identify putative GGA2 binding proteins, four independent BioID experiments were carried out in MDA-MB-231 cells expressing myc-BirA or myc-BirA-GGA2 (Fig. S5A, Table 1). Biotinylated proteins were detected by semi-quantitative spectral counting mass spectrometry method. Proteins with higher number of peptide spectrum matches (PSM) in myc-BirA-GGA2 than myc-BirA in at least 3 experiments were considered as putative GGA2 binders (Table 1). The nine identified proteins included some known GGA2 interactors (ARF6 and IGFR2; Fig. 5A) as well as new putative GGA2 proximal regulators representing potentially new players in integrin traffic. As expected, gene ontology pathway analysis of the putative GGA2 interactors indicated significant enrichment of the trans-Golgi network. In addition, “recycling endosome membrane pathway” was significantly enriched based on 3 proteins (Fig. 5B) ARF6, a known regulator of integrin recycling (Powelka, Sun et al. 2004b) and RAB10 and RAB13 which, to

the best of our knowledge, have not been linked to β1-integrin traffic previously. In the interaction network, RAB13 and RAB10 formed a unique node (dotted box; Fig. 5A). To validate the BioID results, we probed GFP-GGA2 GFP-Trap pulldowns for endogenous RAB10 and RAB13 and found that both of these proteins were expressed in MDA-MB-231 cells and could associate with GFP-GGA2 (Fig. 5C,D). Furthermore, immunofluorescence analyses demonstrated that endogenous RAB13 and GGA2, as well as GFP-RAB13 and GGA2, localise to overlapping perinuclear and plasma membrane-proximal vesicles in MDA-MB-231 cells (Fig. 5E, S5D). This is congruent with the established role of RAB13 function in exocytic membrane traffic from the trans-Golgi network and recycling endosomes to the cell surface in polarized epithelial cells and cancer cells (Nokes, Fields et al. 2008a). While we were unable to identify antibodies for staining endogenous RAB10, we observed overlap between GFP-RAB10 and endogenous GGA2 on perinuclear endomembranes (Fig. 5F). However, unlike RAB13, RAB10 was not detected on the plasma membrane.

RAB10 and RAB13 associate with β1-integrins

Next, we investigated the ability of GGA2 proximal proteins, RAB10 and RAB13, to associate with β1-integrins. Although RAB13 has been implicated in Mst1 kinase-induced delivery of lymphocyte function associated antigen-1 (an immune cell-specific integrin) to the cell surface in lymphocytes, RAB10 and RAB13 have not been linked to the traffic of the ECM-binding α/β1-integrin heterodimers (Nishikimi, Ishihara et al. 2014). We found that both GFP-RAB10 and GFP-RAB13 readily associate with endogenous β1-integrin (Fig. 6A). In cells, GFP-RAB13 localised clearly on large β1-integrin endosomal vesicles and overlapped with β1-integrin on the cell surface (Fig. 6B). In contrast, enrichment of RAB10 to integrin-positive vesicles was less apparent and it did not overlap with β1-integrin on the plasma membrane (Fig. 6B). Furthermore, endogenous RAB13 and β1-integrin colocalised at steady state in MDA-MB-231 cells (Fig. 6C). Taken together, RAB10 and RAB13 represent previously unknown GGA2 proximal proteins that associate with β1-integrins. In addition, RAB13, in particular, exhibits significant overlap with β1-integrins in intracellular vesicles as well as on the plasma membrane.

RAB13 is required for recycling of active β1-integrin

To assess if RAB10 or RAB13 are involved in trafficking of β1-integrins, we first repeated the biotin-IP-based β1-integrin endocytosis assay (Fig. 1A) in cells silenced for RAB10 or RAB13.

Depletion of RAB13 (siRNA#1) significantly increased the level of intracellular β1-integrin following 20 minutes of endocytosis (Fig. 7A,B; Fig. S6A), similarly to GGA2 silencing (Fig. 1A). In contrast, silencing of RAB10 had no significant effect on β1-integrin traffic (Fig. S6B-S6C), suggesting that it may have a role in regulating other GGA2-dependent processes than β1-integrin traffic. Importantly, silencing of GGA2, RAB10 or RAB13 proteins did not influence the protein levels of the other GGA2-proximal components (Fig. S6A,D,E) indicating that their expression/stability are independently regulated and hence silencing influences only the specifically targeted component of this trafficking pathway.

Congruently with the results obtained with GGA2 depletion (Fig. 1-2), silencing of RAB13 significantly increased the uptake of cell-surface-labelled active, but not inactive, β1-integrins in the flow cytometry based internalization assay (Fig. 7C,D). These data were further validated by silencing RAB13 with two independent siRNA and analysing active and inactive β1-integrin internalization from the cell surface using immunofluorescence imaging. Loss of RAB13 resulted in a significant increase in accumulation of active β1-integrin in intracellular vesicles (Fig. 7E,F). Conversely, overexpression of GFP-RAB13 significantly reduced active β1-integrin accumulation inside cells (Fig. 7 G,H) and, in line with GGA2 overexpression (Fig. S2A, B), GFP-RAB13 overexpression had no significant effect on the localization of cell-surface-labelled inactive-β1 integrin (Fig. S7A, B). Inhibition of receptor recycling with primaquine reduced the difference in active β1-integrin internalization between GFP and GFP-RAB13 expressing cells (Fig. S7C,D), indicating that RAB13 influences recycling of active β1-integrin in these cells. Taken together silencing of RAB13 and GGA2 significantly impairs cell-surface targeting of endocytosed active β1-integrin indicating a joint or sequential regulation of active receptor dynamics by these proteins.

Discussion

β1-integrin trafficking plays an important role in the dynamic regulation of cell adhesion and motility and is implicated in malignant processes such as cancer cell invasion (Bridgewater, Norman et al. 2012, De Franceschi, Hamidi et al. 2015). However, the molecular mechanisms and proteins regulating the specificity of integrin traffic remain poorly characterized. Here we have used RNAi screening and BioID to identify new regulators of integrin traffic and demonstrate a role for GGA2, and its previously unknown proximal binding partner RAB13, in the trafficking of active β1-integrins (Fig. 7I).

Our work suggests GGA2 as an important determinant of activity-dependent integrin traffic and hence cancer-related processes, such as cell migration and invasion. We reported previously that GGA3-depletion results in lysosomal targeting and downregulation of collagen binding α2β1-integrin, due to mislocalisation of β1-integrin recycling component SNX17 (Steinberg, Heesom et al. 2012, Bottcher, Stremmel et al. 2012) to late endosomes (Ratcliffe, Sahgal et al. 2016). In contrast, GGA2 is unique in its integrin regulation as it does not affect β1-integrin stability or levels, but instead specifically facilitates the trafficking of active β1-integrins. Increased active β1-integrin accumulation in GGA2-silenced cells is fully reversed upon treatment with the membrane recycling inhibitor drug primaquine, implicating a role of GGA2 in the recycling of active β1-integrin to the plasma membrane.

A role for GGA2 is mediating receptor recycling is surprising since GGA2 has been described to localize to the trans-Golgi network and clathrin-coated vesicles (Dell'Angelica, Puertollano et al. 2000, Puertollano, Randazzo et al. 2001). In addition, a “knocksideways”-depletion indicates a role for GGA2 in anterograde but not retrograde Golgi trafficking (Hirst, Borner et al. 2012). However, the biological role and subcellular localisation of GGA2 has not been studied extensively in carcinoma cells. Focusing on invasive breast cancer MDA-MB-231 cells, where integrin traffic is implicated in the regulation of cell motility (Gu, Noss et al. 2011, Mai, Veltel et al. 2011, Pellinen, Arjonen et al. 2006), we found a subpopulation of GGA2 colocalizing with RAB5 and EEA1 early endosomes, RAB4 and RAB11 recycling endosomes and VPS35 (a component of the retromer), but not with LAMP1 or RAB7 late endosomes. We also detected GGA2 on the plasma membrane, possibly explaining how GGA2 might affect the trafficking of β1-integrins.

Furthermore, we employed BioID proximity biotinylation (Roux, Kim et al. 2012) to define GGA2 proximal proteins in situ in intact MDA-MB-231 cells. We identified two RAB family small GTPases, RAB13 and RAB10, associating with both GGA2 and β1-integrin. Loss-of-function experiments validated a role for RAB13 in the recycling of the active β1-integrin receptor. RAB10, on the other hand, may regulate some other GGA2 and integrin functions, but this remains to be investigated. We also identified known (e.g., IGFR2), as well as new, GGA2 proximal proteins. In our list of interactors (Fig. 5A): we are only displaying the interactors scoring positive in three or more experiments. However, it is interesting to note that three of the recently described proteins affected by knocksideways depletion of GGA2 in HeLa cells (RABEP1, TNFAIP8 and PARP4) (Hirst, Borner et al. 2012) were also identified in our BioID as GGA2 proximal components, but only in 2 out of 4 assays. Thus, while not all of the

identified GGA2 interactors are likely to regulate integrin traffic, they may be vital GGA2 effectors in other yet unknown biological processes.

RABs play important roles in different steps of receptor trafficking and are linked to cancer progression (Subramani, Alahari 2010). Two specific RABs, RAB21 and RAB25, have previously been shown to regulate integrin traffic by directly binding to integrins. RAB21 is widely expressed in different cell types. It recognizes a conserved motif found in the α-tails of all integrins (apart from α11) and regulates integrin endocytosis (Pellinen, Arjonen et al. 2006, Mai, Veltel et al. 2011). RAB25, on the other hand, is expressed only in specific epithelial tissues and some carcinomas (Wang, Hu et al. 2017) and associates with the fibronectin binding α5β1 integrin to drive its recycling (Caswell, Spence et al. 2007). Previous studies have shown the role of RAB13 in trafficking of receptors between trans-Golgi network and transferrin-positive recycling endosomes in epithelial cells (Nokes, Fields et al. 2008b) and activation of RAB13 by guanine nucleotide exchange factor DENND2B on the plasma membrane has been linked to cancer cell migration and invasion (Ioannou, Bell et al. 2015). Thus, RAB13 functions not only in endosomes but also on the plasma membrane. Our identification of a GGA2-RAB13 association reveals a possible mechanism for GGA2 targeting to the plasma membrane in cancer cells. We find that RAB13 silencing impairs active integrin traffic similarly to GGA2 depletion. Moreover, RAB13 also colocalizes with GGA2 and β1-integrin to endosomes and the plasma membrane, suggesting that the previously described RAB13-mediated defects in cancer cell migration and invasion (Ioannou, Bell et al. 2015) may involve the GGA2 and β1-integrin complex.

RAB GTPases are the master regulators of intracellular membrane traffic and are involved in virtually all steps of trafficking including vesicle formation, transport and fusion. There are almost 70 known RABs in humans and dysregulation in the functions of these proteins leads to many diseases including cancer (Stenmark 2009, Hutagalung, Novick 2011). There are still many unknown functions for RABs in membrane trafficking and in human ailments. Furthermore, the role of trafficking adaptors, such as GGAs, is not fully explored in human cancer. Recently, several multiprotein complexes have been assigned as regulators of integrin traffic, including the retriever complex (McNally, Faulkner et al. 2017) and the CORVET complex (Jonker, Galmes et al. 2018). Our data, putting forward a role for a β1-integrin, GGA2 and RAB13 complex in the recycling of active β1-integrins contributes to the view of multi-subunit complexes regulating receptor traffic and contributing to the remarkable sophistication

and specificity of membrane trafficking pathways that determine cellular fitness in a fundamental way.

Acknowledgments

We thank P. Laasola and J. Siivonen for technical assistance, M. Saari for help with the microscopes. We also thank The Cell Imaging Core and Proteomics core facilities at Turku Centre for Biotechnology supported by the University of Turku and Biocenter Finland, for technical assistance with imaging. H. Hamidi for the scientific illustrations and manuscript editing, the Ivaska lab for critical reading and feedback on the manuscript. This study has been supported by the Academy of Finland (J.I.), Academy of Finland CoE for Translational Cancer Research (J.I.), ERC CoG grant 615258, Sigrid Juselius Foundation, Orion Research Foundation and the Finnish Cancer Organization (J.I.). P.S. has been supported by the Turku Doctoral Program of Molecular medicine (TuDMM).

Authors contributions

Conceptualization, J.I.; Methodology, P.S., J.A., A.A., I.P., J.I.; Formal Analysis,.P.S., A.R., A.A., I.P.; Investigation, P.S., J.A., A.A., I.P., M.P. J.I.; Writing– Original Draft, J.I and P.S..; Writing – Review and Editing, J.I., P.S., A.R., J.A.; Visualization, P.S., J.A., I.P. Supervision, J.I.; Funding Acquisition, J.I.

Conflicts of interests

The authors declare no competing financial interests.

Figures, supplementary Figures and Figure legends

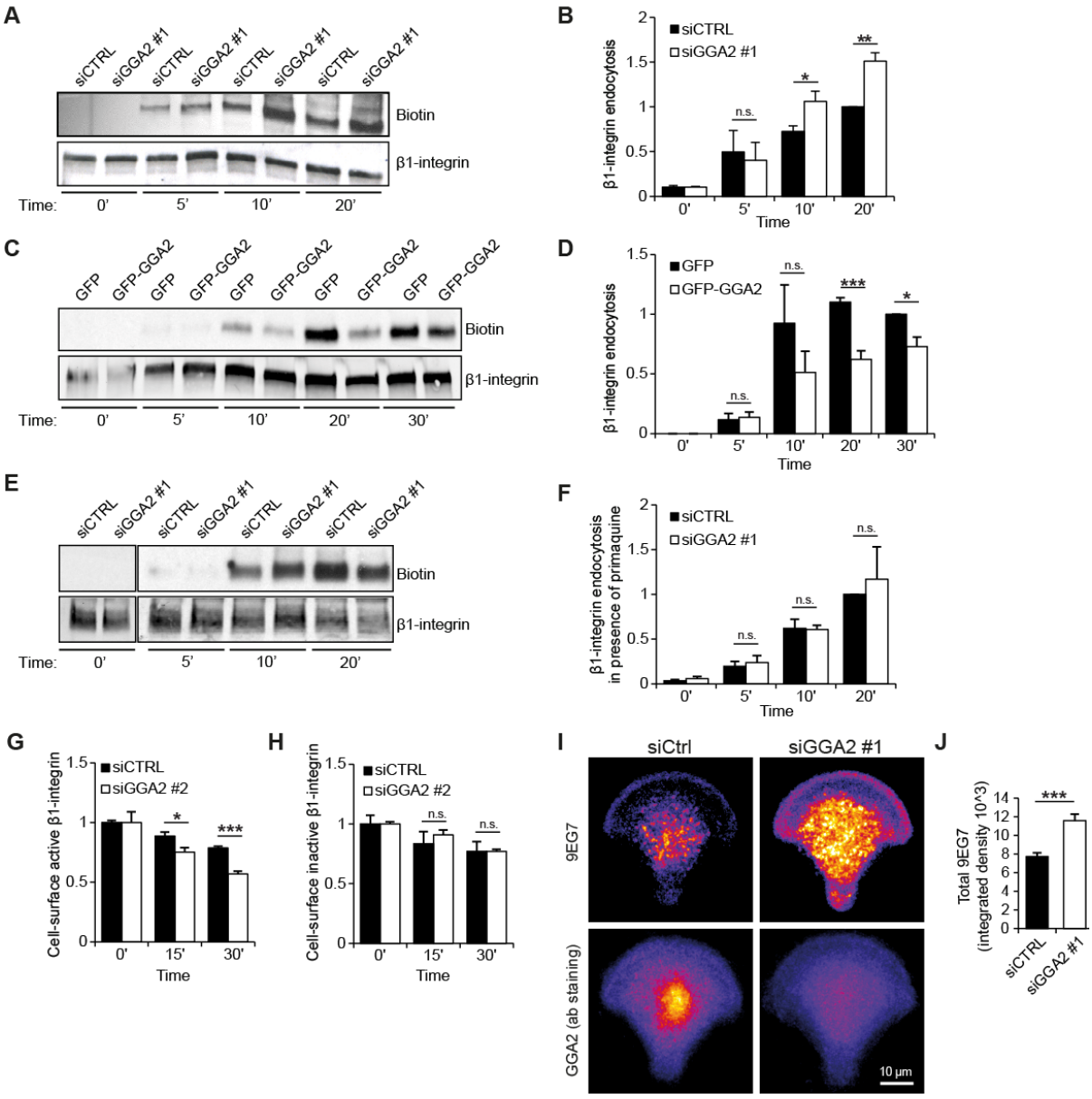

Figure. 1. **GGA2 regulates β1-integrin receptor traffic.**

A-B) Internalization of biotinylated cell-surface β1-integrin in MDA-MB-231 cells treated with either control siRNA (siCTRL) or GGA2 siRNA oligo #1 (siGGA2 #1). Shown is a representative western blot (A) and quantification of biotinylated β1-integrin relative to total β1-integrin levels and normalized to siCTRL 20 min time point (B; data are mean ± SEM of n = 3 independent experiments).

C-D) Internalization of biotinylated cell-surface β1-integrin in MDA-MB-231 cells expressing GFP or GFP-GGA2. Shown is a representative western blot (C) and quantification of biotinylated β1-integrin relative to total β1-integrin and normalized to siCTRL at 20 min time point (D; data are mean ± SEM of n = 3 independent experiments).

E-F) Biotinylation-based integrin internalization assays performed and analysed as in (A, B) with siRNA-treated MDA-MB-231 cells in the presence of the receptor recycling inhibitor primaquine (data are mean ± SEM of n = 3 independent experiments).
G-H) Flow cytometry analysis of cell-surface levels of active (12G10 antibody) (G) or inactive (MAB13 antibody) (H) β1-integrin in siCTRL or siGGA2 #2 (GGA2 siRNA oligo #2) silenced MDA-MB-231 cells following the indicated internalization periods, normalized to siCTRL at 0 min time point (data are mean ± SEM of n = 3 independent experiments).
I-J) Representative mean intensity maps (I) of active β1-integrin immunofluorescence (9EG7) in siCTRL or siGGA2#1 MDA-MB-231 cells plated on fibronectin-coated crossbow-shaped micropatterns. Mean fluorescence intensity of the 9EG7 signal is represented with a heat map (blue, low levels; yellow, high level), where yellow corresponds to regions containing the largest accumulation of active β1-integrin (I). Total levels of active β1-integrin in each condition were also quantified (J; data are mean ± SEM; n=38 cells in each condition).
Statistical analysis, Student's unpaired *t*-test (*p < 0.05, **p < 0.005, ***p < 0.0005).

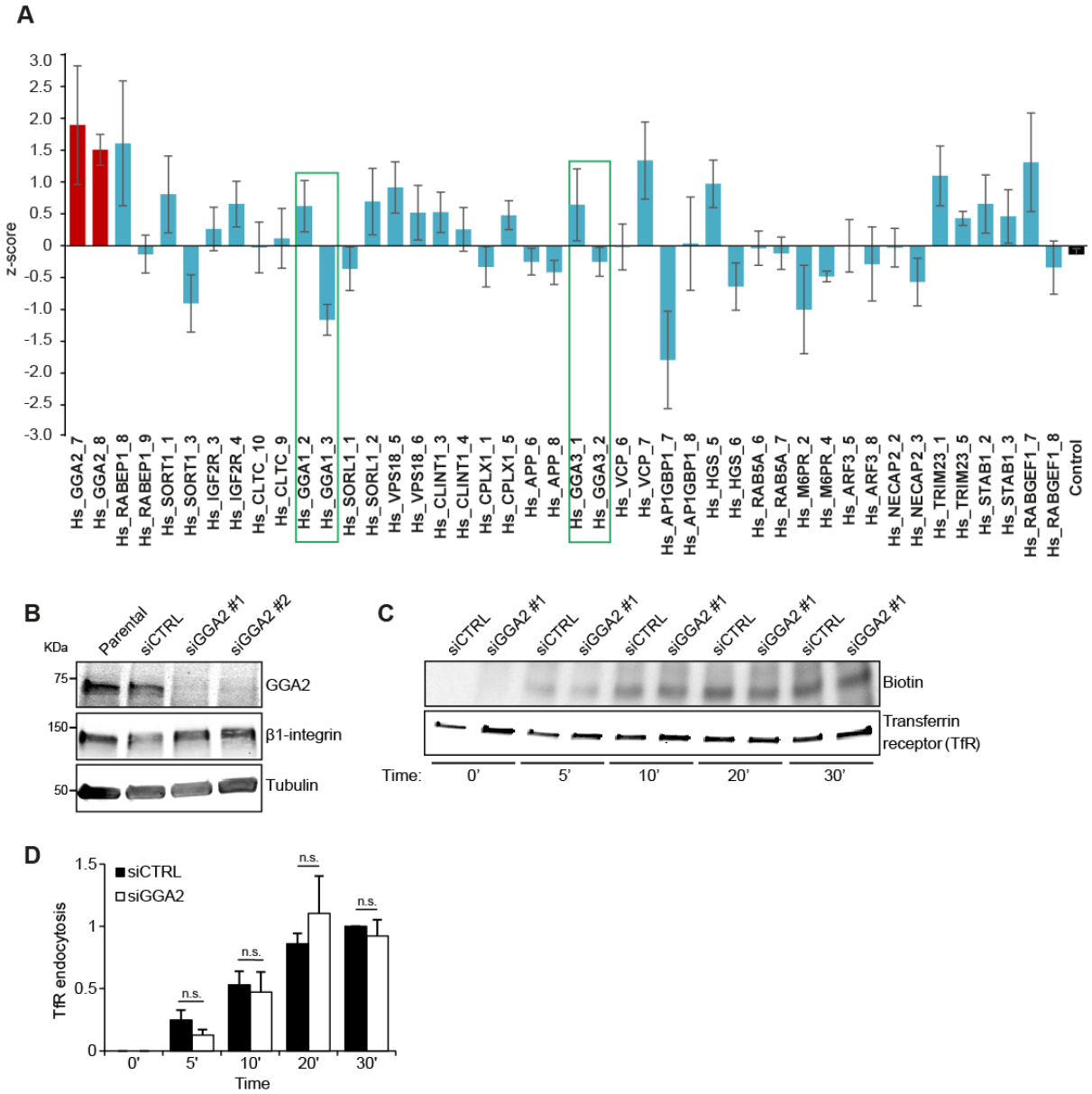

Figure S1. **RNAi screening identifies GGA2 as a regulator of integrin internalization**

A) Differential effects of human GGAs and their known interactors on β1-integrin internalization. After silencing of the indicated genes with two siRNAs using the CSMA platform (see methods), β1-integrin endocytosis was measured using the antibody-based β1-integrin endocytosis assay at 30 min internalization. Endocytosis levels are represented as Z-scores for the whole dataset (red bars: GGA2 siRNAs; green outlines: GGA1 and GGA3 siRNAs; cyan bars: siRNAs against GGA interactors; black bar: control siRNA). Positive z-scores indicate increased internalization of β1-integrin in response to gene silencing. (Data are mean ± SEM; n = 4).

B) Representative western blotting analysis of GGA2 and β1-integrin levels in siCTRL, siGGA2 #1 and siGGA2 #2 MDA-MB-231 cells. Tubulin is included as a loading control.

C-D) Internalization of biotinylated cell-surface transferrin receptor (TfR) in siCTRL or siGGA2 #1 MDA-MB-231 cells. Shown is a representative western blot and quantification of biotinylated TfR relative to total TfR normalized to siCTRL at 30 min time point (data are mean ± SEM of n = 3 independent experiments; statistical analysis, Student's unpaired *t*-test; n.s. = not significant)

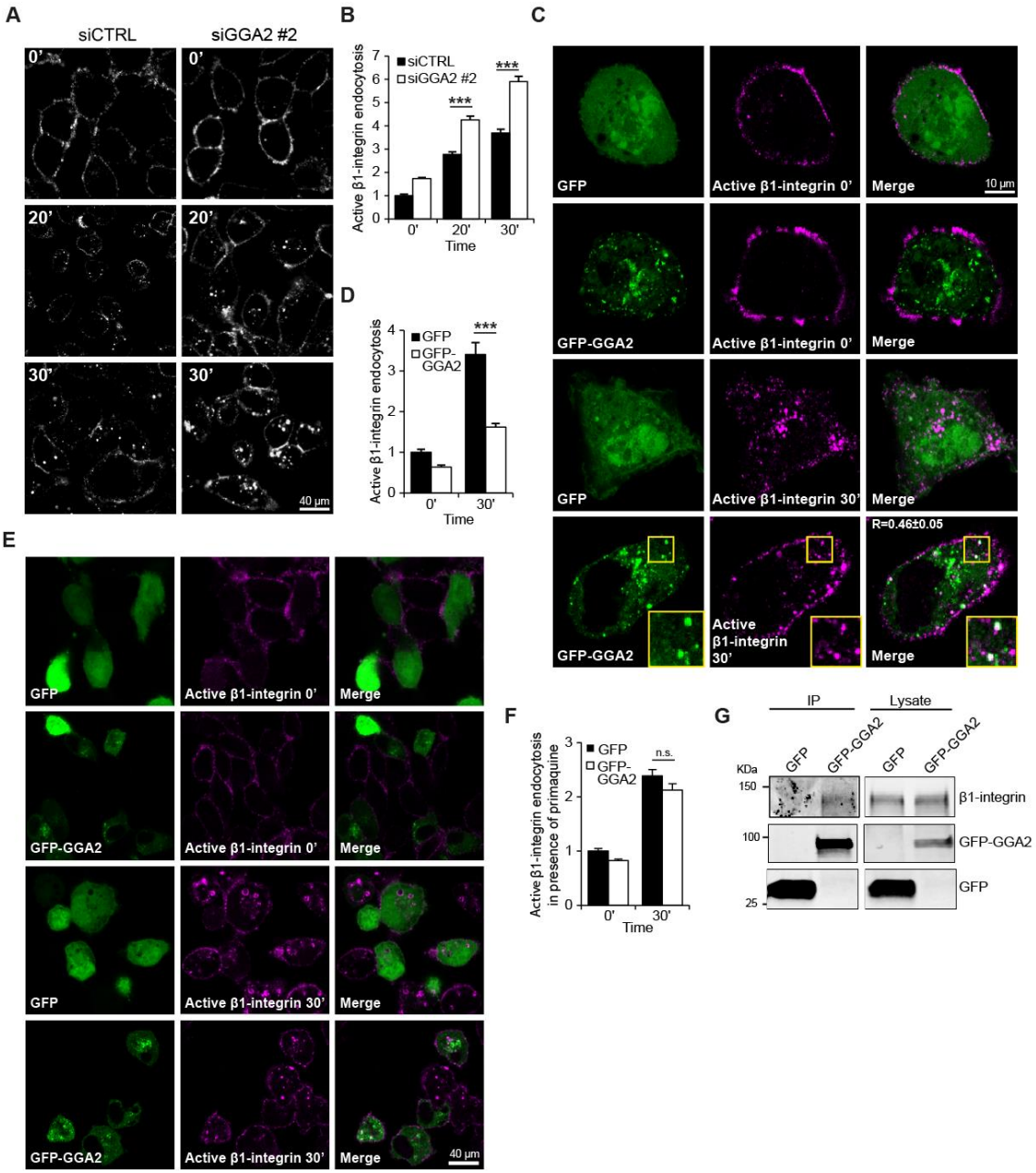

Figure 2. **GGA2 associates with β1-integrins and regulates traffic of active β1-integrins.**
A) Representative confocal microscopy images of active β1-integrin (12G10 antibody) following internalisation, at 37°C, for indicated time points in siCTRL or siGGA2 #2 MDA-MB-231 cells.
B) Quantification of intracellular active β1-integrin levels (12G10 fluorescence signal) from A, normalized to siCTRL at 0 min time point (data are mean ± SEM; n = 100-120 cells per condition).
C) Representative confocal microscopy images of active β1-integrin (12G10 antibody) following internalisation, at 37°C, for the indicated time points in MDA-MB-231 cells expressing GFP or GFP-GGA2. Colocalization of GFP-GGA2 and 12G10 signals (white) is shown in the region of interest (yellow inset) and quantified (R=Pearsons's correlation coefficient between the indicated proteins ± SD; n = 109 cells).

D) Quantification of intracellular active β1-integrin levels (12G10 fluorescence signal) from C, normalized to GFP MDA-MB-231 cells at 0 min time point (data are mean ± S.E.M; n = 70-110 cells per condition).
E) Representative images of active β1-integrin (12G10 antibody) following internalisation, at 37°C, for the indicated time points in MDA-MB-231 cells expressing GFP or GFP-GGA2 and treated with 100 µM primaquine.
F) Quantification of intracellular active β1-integrin levels (12G10 fluorescence signal) from E, normalized to GFP MDA-MB-231 cells at 0 min time point (data are mean ± SEM; n = 70-80 cells per condition).
G) Representative western blotting analysis of endogenous β1-integrin and GFP levels in GFP-TRAP pulldowns performed in GFP or GFP-GGA2 expressing MDA-MB-231 cells (n = 3 independent experiments).
Statistical analysis, Student's unpaired *t*-test **(**n.s.= not significant, ***p < 0.0005).

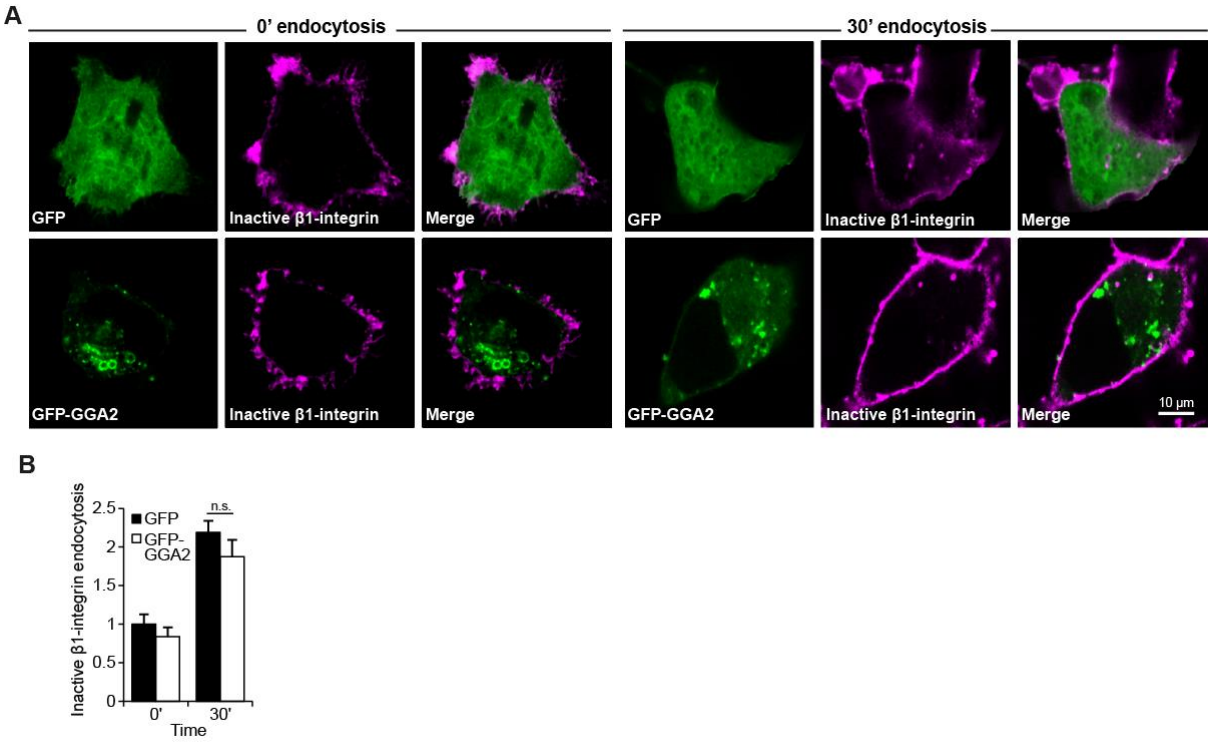

Figure S2. **GGA2 does not influence traffic of inactive β1-integrins**
A) Representative confocal images of inactive β1-integrin (MAB13 antibody) following internalisation, at 37°C, for the indicated time points in MDA-MB-231 cells expressing GFP and GFP-GGA2.
B) Quantification of intracellular inactive β1-integrin (MAB13 fluorescence signal) from A, normalized to GFP MDA-MB-231 cells at 0 min time point (data are mean ± SEM; n = 70-110 cells per condition).
Statistical analysis, Student's unpaired *t*-test **(**n.s.= not significant)

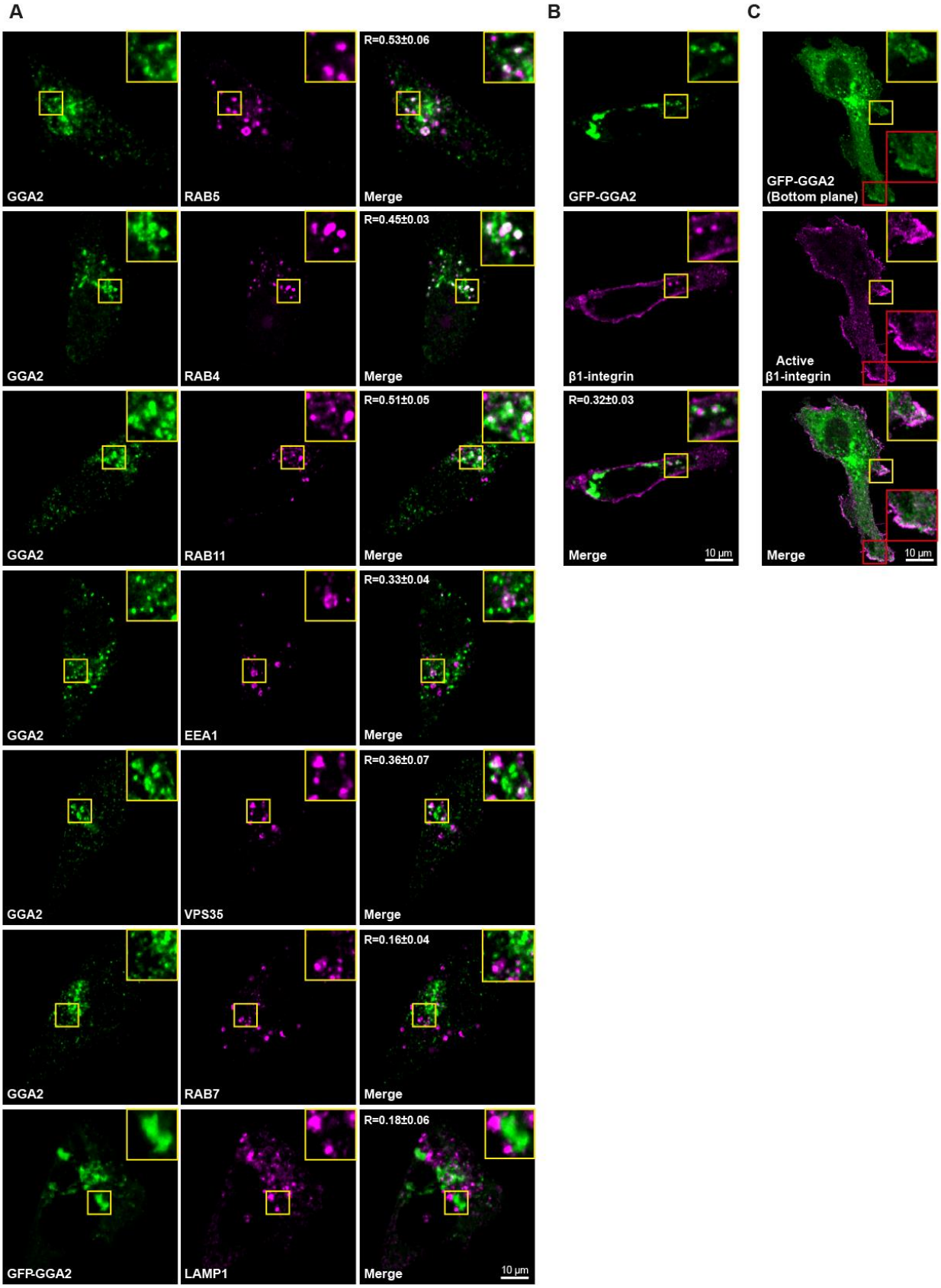

Figure 3. **Cellular characterization of GGA2 localisation**

A-B) Representative confocal microscopy images of MDA-MB-231 cells stained for the indicated vesicular compartment proteins (magenta) with either endogenous GGA2 or GFP-GGA2 (green). Colocalization in white (yellow inset) and quantified (R=Pearsons's correlation coefficient between the indicated proteins ± SD; n = 80-200 cells per condition).
C) Representative microscopy images (bottom confocal plane) of GFP-GGA2 (green) and 12G10 (magenta).

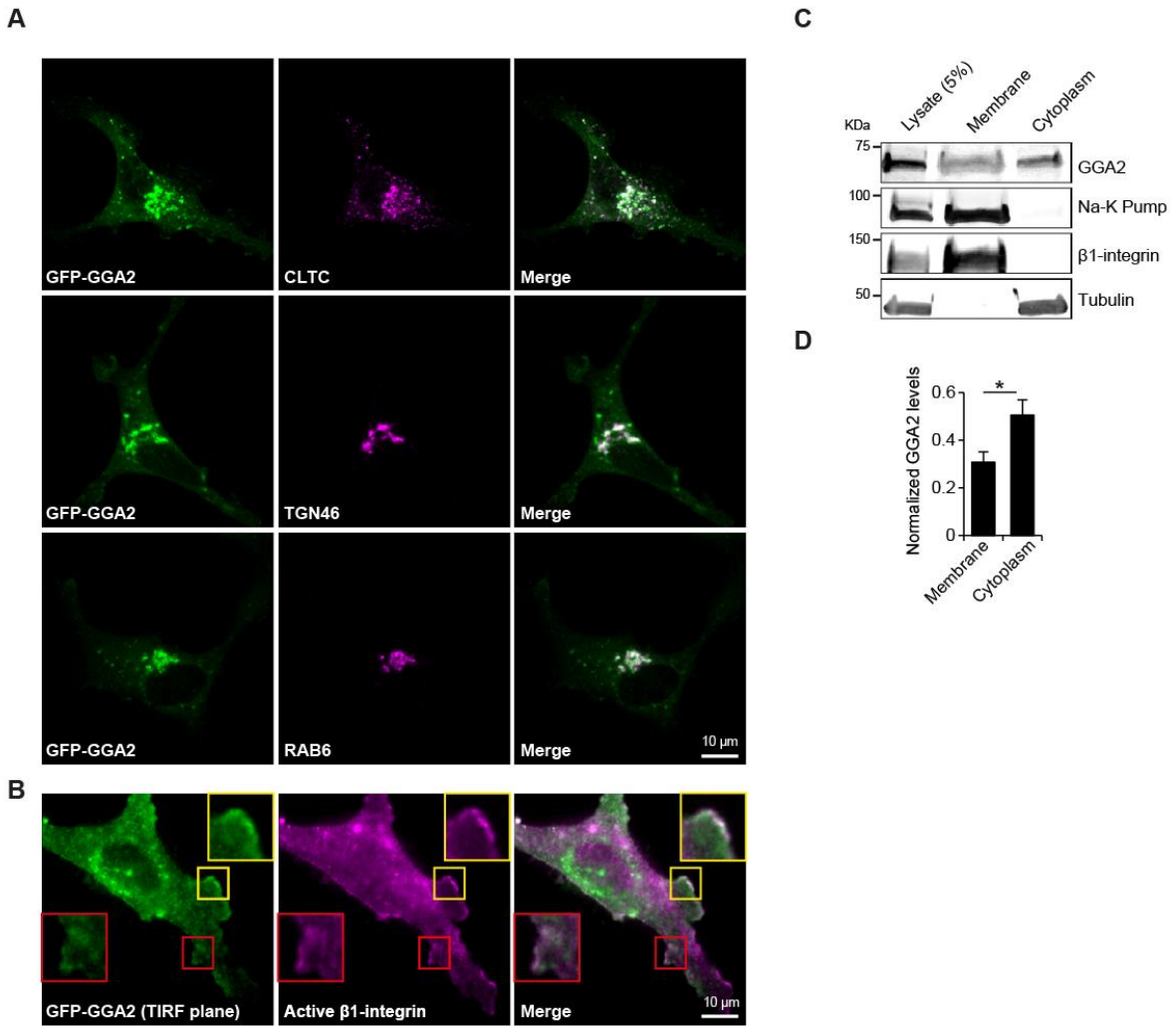

Figure S3. **GGA2 colocalises to the trans-Golgi and the plasma membrane**
A) Representative confocal microscopy images of MDA-MB-231 cells stained for the indicated intracellular compartment proteins (magenta) with GGA2-GFP (green). Colocalization in white (yellow inset).
B) Representative TIRF microscopy images of GGA2-GFP (green) and active β1-integrin (12G10, magenta). Colocalization in white (yellow inset).
C) Subcellular fractionations of MDA-MB-231 using differential centrifugation and analysis of GGA2 expression in the membrane and cytosolic fractions. A representative western blot is shown, where β1-integrin and Na+-K+ pump were blotted as positive controls for the

membrane fraction and tubulin for the cytosolic fraction. The total cell lysate is included as a loading control.

D) Quantification of GGA2 subcellular localization from C (data are mean ± SEM, n = 3 independent experiments; statistical analysis: Student's unpaired *t*-test, *p < 0.05**).**

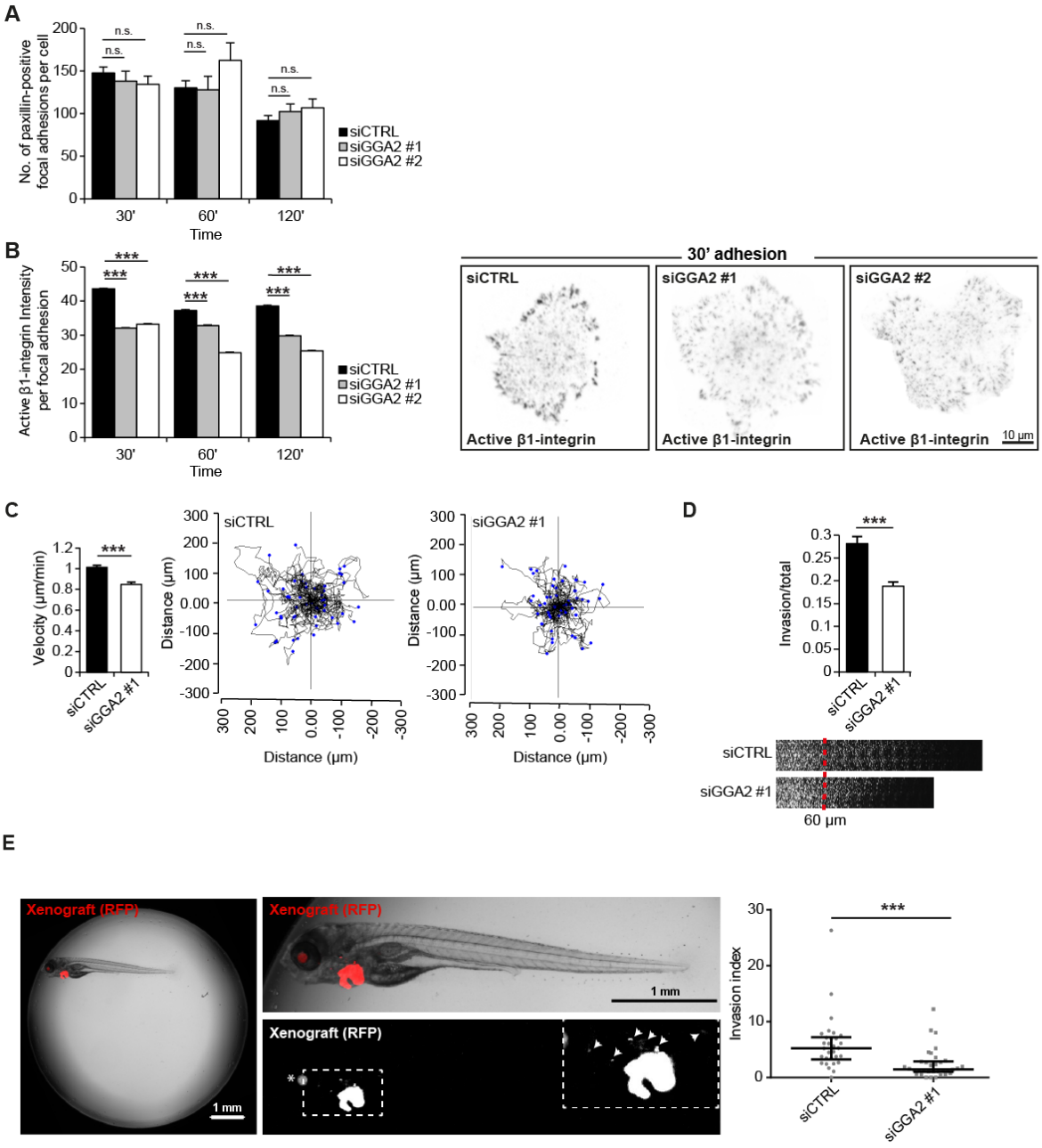

Figure 4. **GGA2 regulates active β1-integrin in focal adhesions, cell migration and cancer cell invasion.**

A-B) siCTRL, siGGA2 #1 or siGGA2 #2 MDA-MB-231 cells were plated on collagen and fibronectin for the indicated time points, fixed and stained for paxillin (to detect FA number) and active β1-integrin (12G10). Shown are quantifications of focal adhesion number (A) and 12G10 mean fluorescence intensity in focal adhesions with representative confocal microscopy

images (bottom plane) (B) (data are mean ± SEM; n = 7,700-15,700 focal adhesions from 80-110 cells per condition).
C) Quantification of cell velocity in siCTRL or siGGA2 #1 MDA-MB-231 cells migrating randomly on fibronectin-coated dishes (data are mean ± SEM; n = 150-180 cells for each condition). Representative migration tracks are shown in black for 50 cells per condition. End points are represented by blue dots.
D) Inverted invasion assay showing reduced MDA-MB-231 cell invasion following GGA2 silencing. Invasion in collagen plugs supplemented with fibronectin was visualized using confocal microscope by imaging serial optical sections at 15 μm intervals. Individual confocal images are shown in sequence with increasing penetrance from left to right. The invasion was quantified using ImageJ by measuring the fluorescence intensity of cells invading 60 μm relative to the fluorescence intensity of all cells in the plug (data are mean ± SEM, n = 3 independent experiments).
E) Invasion of siCTRL or siGGA2 #1 MDA-MB-231 cells expressing GFP or RFP in zebrafish embryos. Cells were transplanted into the pericardial cavity of 2-day old zebrafish embryos and after 4 days the invasion index of the tumours was measured. Example pictures are from siCTRL MDA-MB-231 tumour xenografts expressing RFP. Magnified region is outlined with a dashed line, invading tumour cells are labelled with arrow heads and non-specific fluorescence in the lens with an asterisk (*) (data are median and interquartile range and individual points are shown as grey dots. siCTRL, n = 30 embryos; siGGA2, n = 35 embryos from two independent experiments).
Statistical analysis: A-D, Student's unpaired *t*-test **(**n.s.= not significant, ***p < 0.0005); E, non-parametric Mann-Whitney test (***p <0.0001).

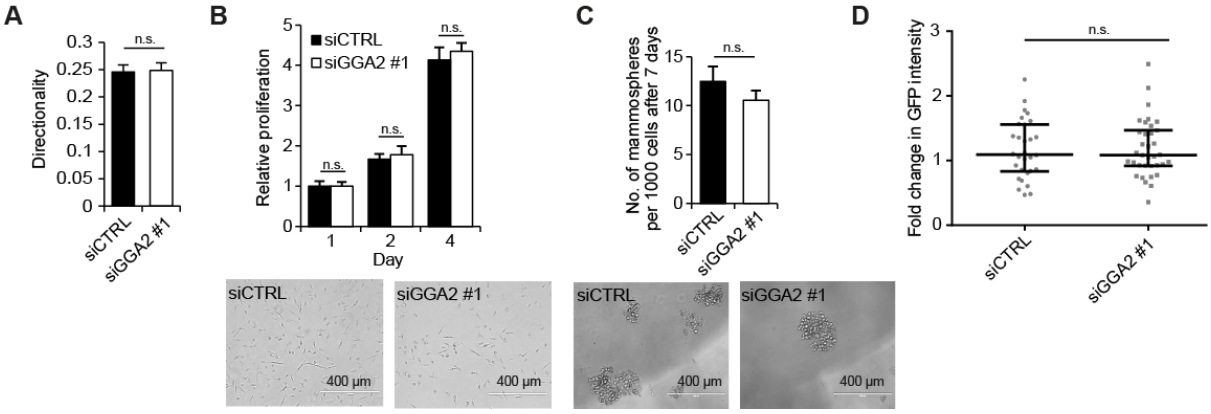

Figure S4. **GGA2 silencing does not influence directionality or cell proliferation**
A) Quantification of cell directionality in siCTRL or siGGA2 #1 MDA-MB-231 cells migrating randomly on fibronectin-coated dishes (data are mean ± SEM; n = 150-180 cells for each condition).
B) Quantification of siCTRL or siGGA2 #1 MDA-MB-231 cell proliferation over 4 days (data are mean ± SEM; n=3 independent experiments). Images show cells at day 4.

C) Quantification and representative images of the number of tumour spheres formed by siCTRL or siGGA2 #1 MDA-MB-231 cells (data are mean ± SEM; n = 3 independent experiments).
D) Relative tumour growth in zebrafish embryos. siCTRL or siGGA2 #1 MDA-MB-231 cells labelled with GFP were transplanted into the pericardial cavity of zebrafish embryos as in 4E and GFP intensity (this was used as an indication of xenograft size) was measured at 1 and 4 days post injection (data are median and interquartile range and individual points are shown as grey dots. siCTRL, n = 30 embryos; siGGA2, n = 35 embryos).
Statistical analysis: A-C, Student's unpaired *t*-test **(**n.s.= not significant); D, non-parametric Mann-Whitney test (n.s. , p =0.8674).

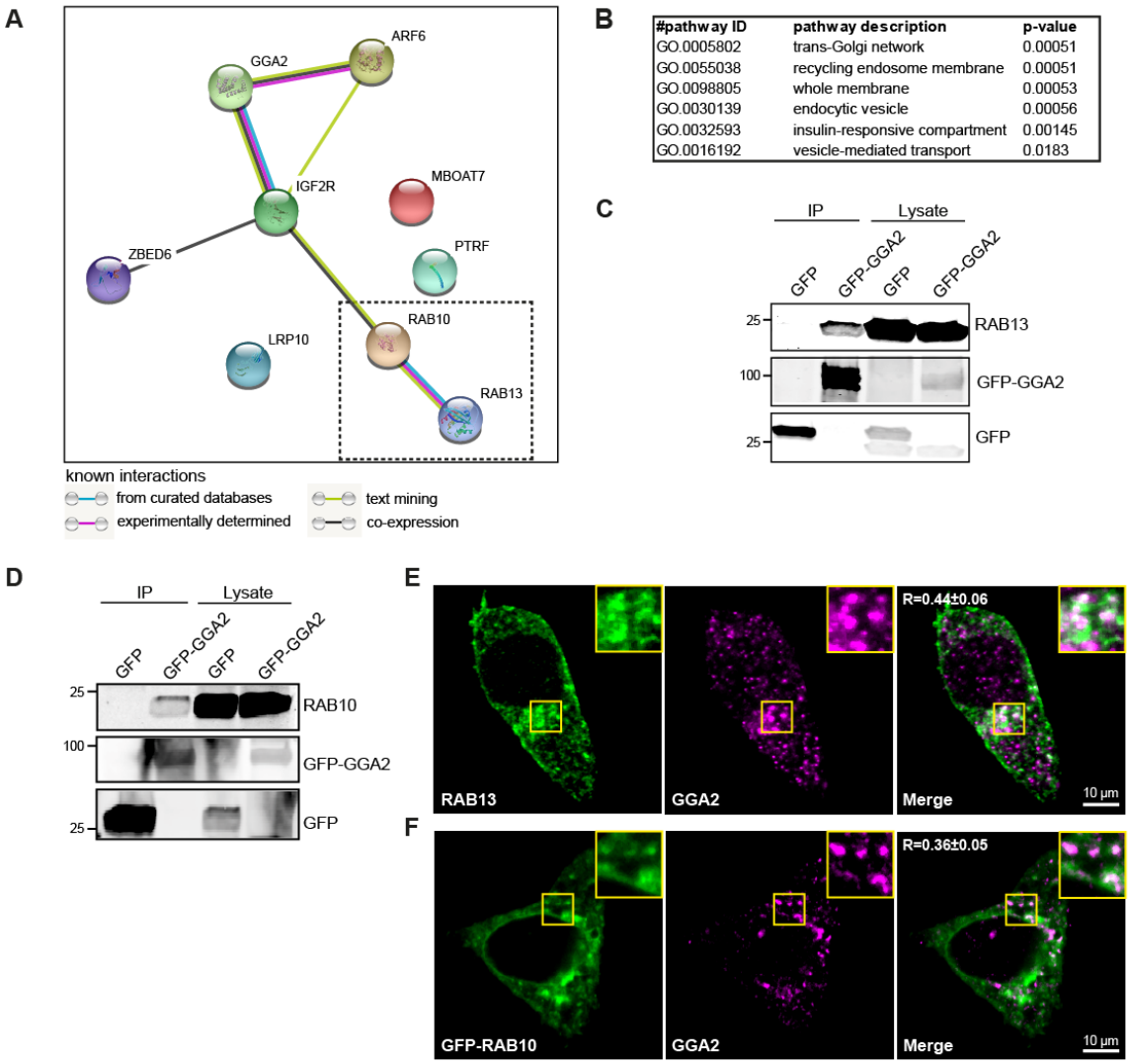

#pathway ID	pathway description	p-value
GO.0005802	trans-Golgi network	0.00051
GO.0055038	recycling endosome membrane	0.00051
GO.0098805	whole membrane	0.00053
GO.0030139	endocytic vesicle	0.00056
GO.0032593	insulin-responsive compartment	0.00145
GO.0016192	vesicle-mediated transport	0.0183

Figure 5. **Proximity biotinylation identifies new GGA2-associated trafficking proteins.**
A) Interaction network of putative GGA2 proximal proteins identified with BioID created by STRING server using medium stringency (confidence 0.200). The node of interest indicated with a dotted outline.

B) Gene ontology analysis created by STRING server of the proteins depicted in (A). p-values indicate for false discovery rate provided by STRING.
C-D) Representative immunoblots of GFP-TRAP pulldowns from MDA-MB-231 cells transiently transfected with GFP or GFP-GGA2 and blotted for GFP and endogenous RAB13 (C) or RAB10 (D) (n = 3 independent experiments).
E-F) Representative confocal microscopy images of MDA-MB-231 cells stained for endogenous RAB13 and GGA2 (E) or transfected with GFP-RAB10 and stained for GGA2. Colocalization in white (yellow insets) and quantified (R = Pearsons's correlation coefficient between the indicated proteins ± SD; n = 80-200 cells per condition).

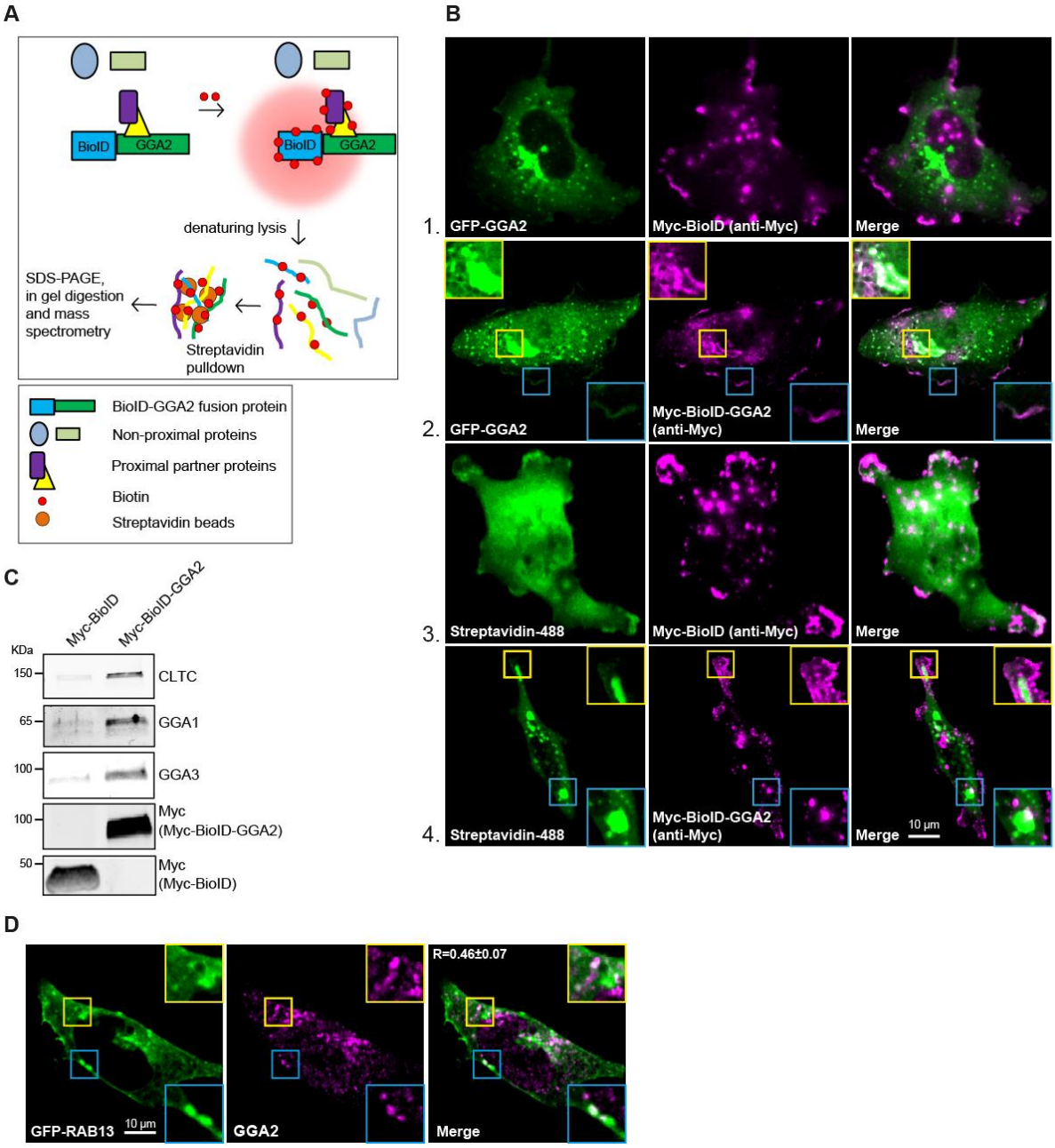

Figure S5. **Controls for the GGA2-BioID**
A) Outline of our BioID approach to detect new GGA2-associating proteins.

B) Representative confocal microscopy images of MDA-MB-231 cells co-transfected with GFP-GGA2 and Myc-BioID (1) or with GFP-GGA2 and Myc-BioID-GGA2 (2). Cytosolic overlap (white) in yellow inset and membrane overlap (white) in the blue inset. MDA-MB-231 cells were also transfected with Myc-BioID or Myc-BioID-GGA2 in the presence of 50 µM biotin (3 and 4, respectively) and stained with anti-streptavidin-alexafluor488 conjugated antibody. Specific compartmentalized overlap (white) between Myc-BioID-GGA2 and streptavidin- alexafluor488 is shown in the yellow and blue insets.
C) Streptavidin pulldown in MDA-MB-231 cells transiently transfected with Myc-BioID or Myc-BioID-GGA2, treated with biotin and lysed. Immunoblotting for known GGA2 interactors (clathrin heavy chain CLTC, GGA1, GGA2) and myc tag is shown.
D) Representative confocal microscopy images of MDA-MB-231 cells transfected with GFP-RAB13 and stained with β1-integrin antibody P5D2. Colocalisation in the cytosol (white) is shown in the yellow inset. Colocalization in white (blue inset) and quantified (R = Pearsons's correlation coefficient between the indicated proteins ± SD; n = 150 cells).

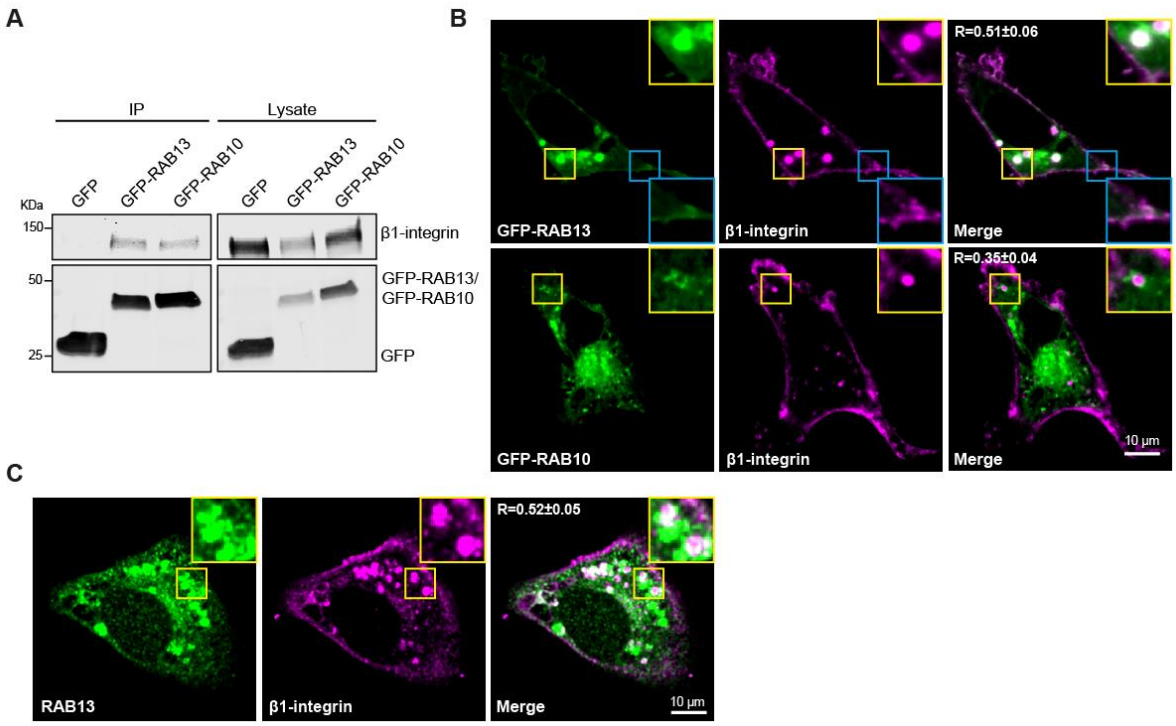

Figure 6. **RAB10 and RAB13 associate with β1-integrins**
A) Representative immunoblots of GFP-TRAP pulldowns from MDA-MB-231 cells transiently transfected with GFP, GFP-RAB10 or GFP-RAB13 and blotted for GFP and endogenous β1-integrin (n=3 independent experiments).
B) Representative confocal microscopy images of MDA-MB-231 cells transfected with GFP-RAB13 or GFP-RAB10 and stained with anti-β1-integrin antibody P5D2. Cytosolic overlap (white) is shown in the yellow inset and colocalisation on the membrane (white) in the blue inset and membrane colocalisation quantified. (R=Pearsons's correlation coefficient between the indicated proteins ± SD, n = 60-100 cells per condition).

D) Representative confocal microscopy images of MDA-MB-231 cells stained for endogenous RAB13 and β1-integrin. Colocalisation in white in the yellow inset and quantified. (R=Pearsons's correlation coefficient between the indicated proteins ± SD, n = 150 cells per condition).

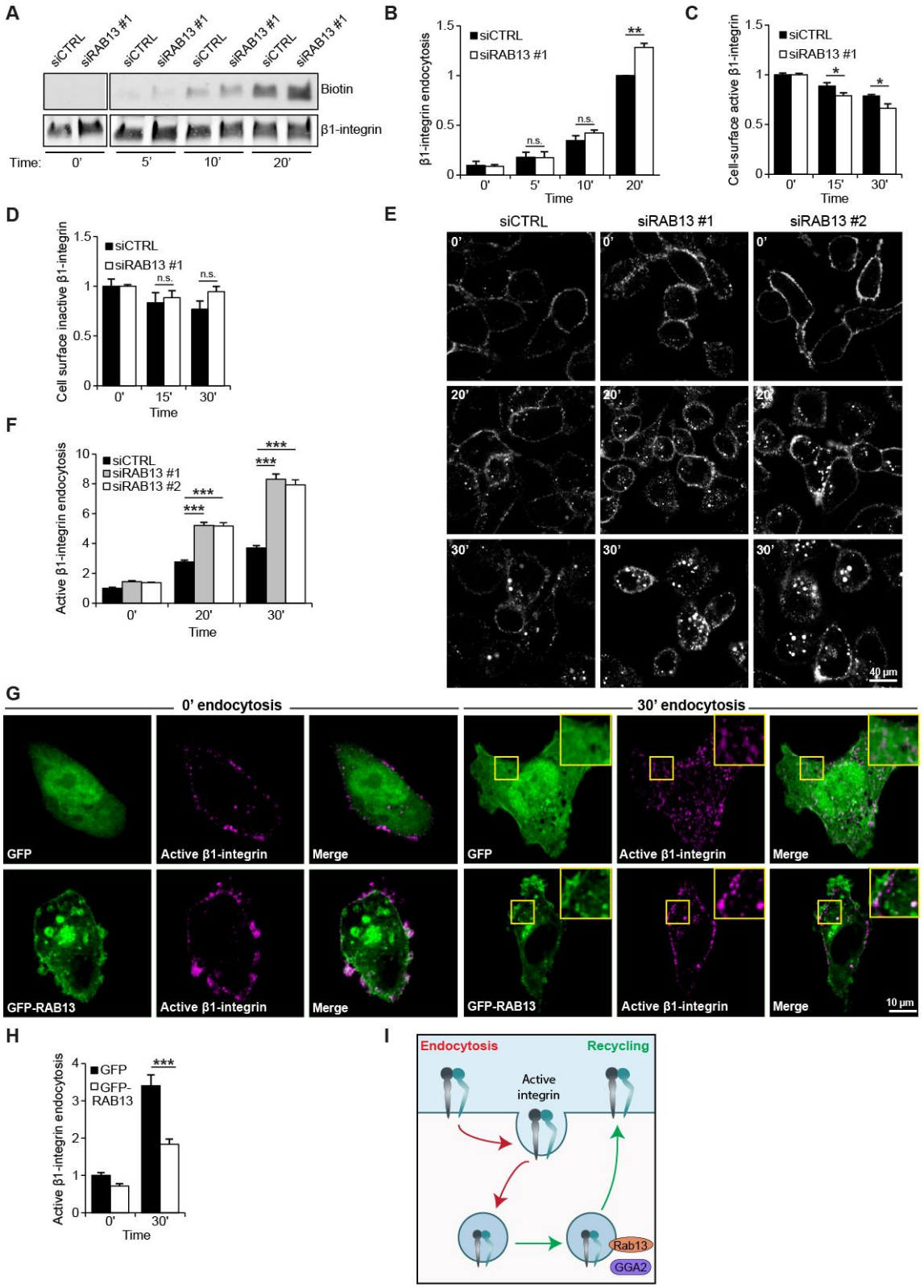

Figure 7. **RAB13 is required for recycling of active β1-integrin**

A-B) Internalization of biotinylated cell-surface β1-integrin in siCTRL or siRAB13#1 MDA-MB-231 cells. Shown is a representative western blot and quantification of biotinylated β1-

integrin relative to total β1-integrin and normalized against siCTRL 20 min time point (data are mean ± SEM of n = 3 independent experiments).
C-D) Flow cytometry analysis of cell-surface levels of active (12G10 antibody) (C) or inactive (MAB13 antibody) β1-integrin (D) in siCTRL or siRAB13#1 silenced MDA-MB-231 cells following the indicated internalization periods, normalized to siCTRL at 0 min time point (data are mean ± SEM of n = 3 independent experiments).
E) Representative images of confocal microscopy based internalization of cell surface labelled active β1-integrin antibody (12G10) at 37°C for indicated time points in control siRNA or RAB13 siRNA#1 or RAB13 siRNA#2 silenced MDA-MB-231 cells.
F) Mean intensity quantification of intracellular 12G10 fluorescence signal. Normalized to 0 min control siRNA time point. (Data are mean±SEM.; n=100-120 cells per condition).
G) Representative images of confocal microscopy based internalization of cell surface labelled active β1-integrin antibody (12G10) at 37°C for 0 min and 30 min in GFP and GFP-RAB13 transiently transfected cells. Yellow insets show higher magnifications of regions of interest.
H) Mean intensity quantification of the intracellular 12G10 fluorescence signal. Normalized to 0 min GFP transfected cells. (Data are mean±SEM.; n=65-220 cells per condition).
Statistical analysis for quantifications **(**n.s.= not significant, $^{*}p < 0.05$, $^{**}p < 0.005$, $^{***}p < 0.0005$. student's unpaired *t*-test**).**

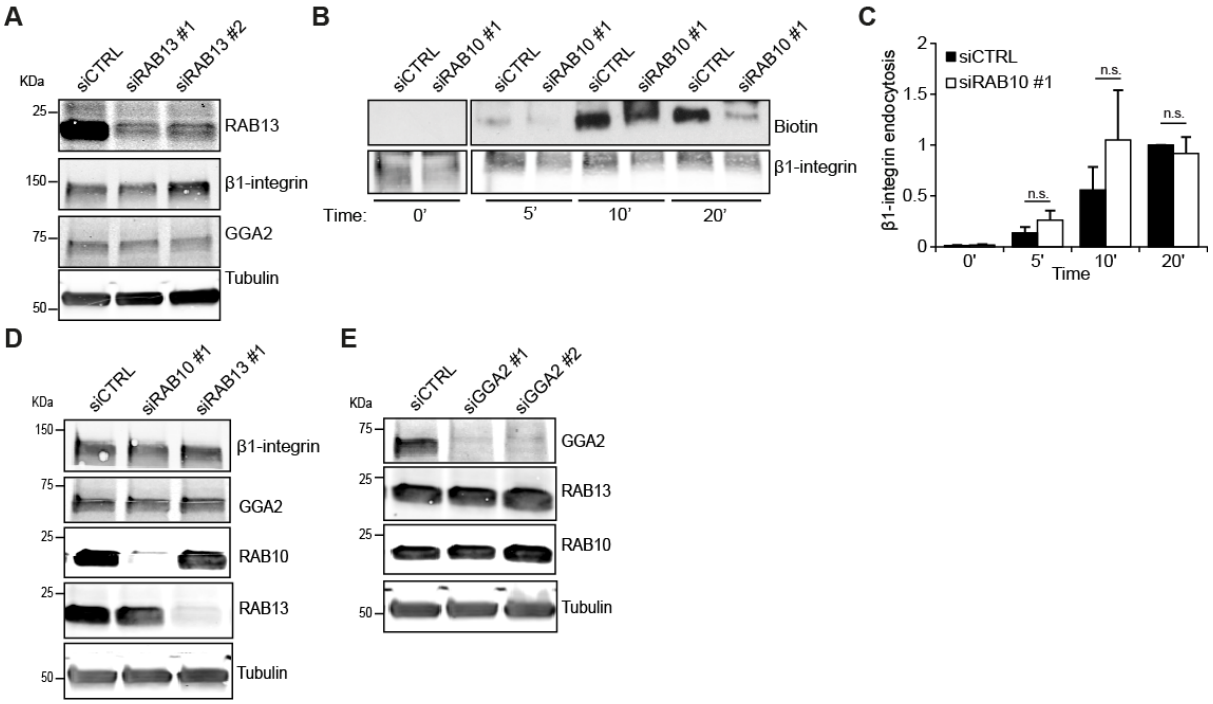

Figure S6. **RAB10 does not regulate β1-integrin traffic**
A) Representative immunoblots of MDA-MB-231 cells silenced with control siRNA, RAB13 siRNA#1 or RAB13 siRNA#2 and blotted for β1-integrin and GGA2. Tubulin as a loading control.
B-C) Internalization of biotinylated cell-surface β1-integrin in control siRNA or RAB10 siRNA silenced MDA-MB-231 cells. Shown is a representative western blot and quantification

of biotinylated β1-integrin relative to total β1-integrin and normalized against 20 min siCTRL time point (data are mean±SEM of n = 3 independent experiments).
D) Representative immunoblots of MDA-MB-231 cells silenced with control siRNA, RAB10 siRNA#1 or RAB13 siRNA#1 and blotted as indicated. Tubulin as a loading control.
H) Representative immunoblots of MDA-MB-231 cells silenced with control siRNA, GGA2 siRNA#1 or GGA2 siRNA#2 and blotted as indicated. Tubulin as a loading control.
Statistical analysis for quantifications **(**n.s.= not significant, student's unpaired *t*-test**).**

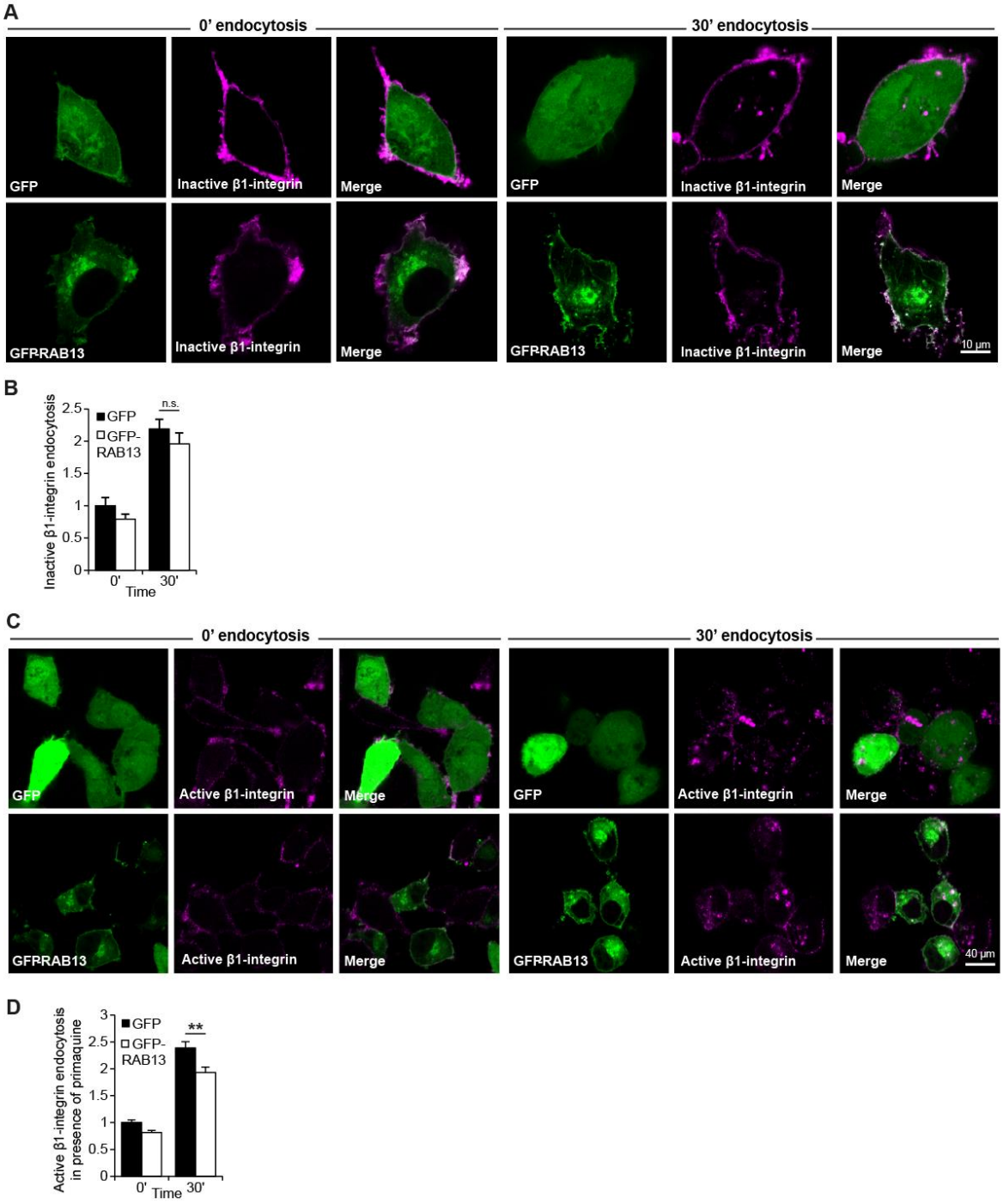

Figure S7. **RAB13 does not influence traffic of inactive β1-integrin**

A) Representative images of confocal microscopy based internalization of cell surface labelled inactive β1-integrin antibody (MAB13) at 37°C for 0 min and 30 min in GFP and GFP-RAB13 transfected MDA-MB-231 cells.
B) Mean intensity quantification of the intracellular MAB13 fluorescence signal. Normalized to GFP transfected cells 0 min time point. (Data are mean±SEM.; n=55-110 cells per condition).
C) Representative images of confocal microscopy based internalization of cell surface labelled active β1-integrin antibody (12G10) at 37°C for 0 min and 30 min and treated with 100 μm primaquine in GFP and GFP-RAB13 transfected MDA-MB-231 cells.
D) Mean intensity quantification of the intracellular 12G10 fluorescence signal. Normalized to GFP transfected cells 0 min time point. (Data are mean±SEM.; n=70-80 cells per condition).
Statistical analysis for quantifications **(**n.s.= not significant, $^{**}p < 0.005$, student's unpaired *t*-test).

Materials and methods

RNAi Screening

Cell Spot Microarrays (CSMA) were conducted as previously described (Rantala et al., 2011). GGA family member and interactor targeting siRNAs (Oligo IDs indicated in Fig. S1A) and control siRNA were purchased from Qiagen. Before plating MDA-MB-231 cells on CSMA, the arrays were blocked with Lutrol F108 (Univar AB) for 15 min at room temperature. Cells were washed and harvested using HyQTase (HyClone, SV30030.01), then plated on CSMA and endocytosis was measured 72 h after the reverse siRNA transfection using an antibody-based β1-integrin endocytosis assay described previously (Arjonen et al., 2012). In short, non-function blocking β1-integrin antibody (K20) was labelled using an AlexaFluor 488 protein labelling kit (Invitrogen). Cells plated in the CSMA were then incubated live with the K20-AlexaFluor 488 conjugated antibody for 1 h on ice to allow labelling of cell-surface integrins. The CSMA was then washed and endocytosis of cell-surface labelled β1-integrins triggered by incubating cells at 37°C for 30 min. Any residual cell-surface fluorescence was then quenched using anti-AlexaFluor 488 antibody (Invitrogen) for 1 h on ice and cells were then fixed using 4% paraformaldehyde, permeabilized and incubated with anti-mouse AlexaFluor 555 secondary antibody to label both internal and cell surface K20 pools (total β1-integrin). Levels of detected endocytosed β1-integrin were normalized against total β1-integrin levels. Nuclei were labelled using Syto60 (Invitrogen). Fluorescence intensities were measured using Laser microarray scanner (Tecan LS400) and ArrayPro Analyzer v4.5 software.

Zebrafish xenograft and metastasis assay

Experiments were performed as described in (Pekkonen, Alve et al. 2018) under license ESAVI/9339/04.10.07/2016. Briefly, adult zebrafishes of casper (roy-/-, mitfa-/- strain) (White, Sessa et al. 2008) were placed into mating tanks and after natural spawning, the embryos were collected for experiments and cultured in E3-medium (5 mM NaCl, 0.17 mM KCl, 0.33 mM $CaCl_2$, 0.33 mM $MgSO_4$) supplemented with 0.2 mM phenylthiourea (PTU, Sigma-Aldrich) at 33°C. After two days of incubation, the embryos were anesthetized (MS-222, 200 mg/l, Sigma-Aldrich) and mounted into 0.7% low-melting point agarose for tumour transplantation. Prior to transplantation, siRNA-treated MDA-MB-231 GFP or MDA-MB-231-RFP cells were trypsinized, washed with PBS and resuspended into injection buffer. Approximately 5–10 nl of cell suspension was microinjected into the pericardial cavity of the embryo using CellTramVario (Eppendorf), Injectman Ni2 (Eppendorf) micromanipulator and

glass needles. After transplantation, the embryos were released from the agarose and cultured in E3-PTU at 33°C. On the next day, successfully xenografted healthy embryos were selected and placed into 96-well plates (1 embryo per well) and imaged with Nikon Eclipse Ti2 microscope equipped with Plan UW 2x objective. At four days post-injection (dpi) the embryos were anaesthetized and imaged again.

The GFP or RFP (referred as FP) intensity of the tumour was measured manually using FIJI software after background subtraction (rolling ball radius = 25) using FIJI (ImageJ version 1.49 k) (Schindelin, Arganda-Carreras et al. 2012). The invasion index was calculated as a ratio of the number of invaded cells relative to the FP fluorescence intensity of the primary tumour at 4 dpi. The relative growth of the primary tumour was calculated by dividing FP intensity at 4 dpi by the FP intensity at 1 dpi. Invading cells in the lens were not counted as these sites often autofluoresce. Significantly malformed, dead or poorly oriented embryos were excluded from the analysis. Samples were not blinded for imaging and subsequent analyses.

Cell culture

MDA-MB-261 cells (ATCC) were grown in Dulbecco's modified essential medium (DMEM; Sigma-Aldrich, D5769) supplemented with 10% fetal bovine serum (FBS; Sigma-Aldrich, F7524), 1% penicillin/streptomycin (Sigma-Aldrich, P0781-100ML), 1% MEM non-essential amino acids (Sigma-Aldrich, M7145) and 1% L-glutamine (Sigma-Aldrich, G7513-100ml). Cells were regularly tested for mycoplasma infection and were grown at +37°C, 5% CO_2, until 70-80 % confluence before washing with PBS (Sigma-Aldrich, D8537), detaching with trypsin (Sigma-Aldrich, T4174-100ML) and plating onto new dishes.

Transient transfections

DNA construct and siRNA transfections were carried out using Lipofectamine 3000 (Invitrogen, L3000-015) and Lipofectamine RNAiMAX (Invitrogen, 13778-150), respectively, according to the manufacturer's instructions. Cells were transfected with DNA constructs for 24 h or with siRNAs for 72 h before the experiment. The siRNAs used in this study are indicated in the reagent table.

Recombinant DNA

GFP-GGA2 and myc-BioID-GGA2 constructs were generated by cloning Human GGA2 from GGA2 ORF entry vector (RC200153, origene) into pTagGFP2-C (FP191, Evrogen) and pcDNA3.1 mycBioID (35700, Addgene) destination vectors respectively using cloneEZ. GFP-

RAB10 and GFP-RAB13 constructs were generated using the Genome Biology Unit cloning service (Biocenter Finland, University of Helsinki). Briefly, GFP entry clone from the human ORFeome collaboration library (RAB10, 100066678; RAB13, 100002881) was transferred into the pcDNA6.2/N-emGFP destination vector using the standard LR reaction protocol.

Western blot analysis

Reduced and heat-denatured protein extracts were separated by SDS-PAGE (4–20% Mini-4–20% Mini-PROTEAN® TGX™ Gel, Biorad, 456-1094) and then transferred onto 0.2 µm nitrocellulose membranes (Trans-Blot Turbo Transfer Pack; Biorad, 170-4158). Membranes were blocked with blocking buffer (Thermo Scientific™ Pierce™ StartingBlock™; 10108313) for 30 min at room temperature and incubated with primary antibodies (see key resources table) diluted in blocking buffer overnight at +4°C with agitation. On the following day, membranes were washed three times with TBST for 10 min each and incubated with the appropriate fluorophore-conjugated secondary antibodies (see key resources table) (1:5000, diluted in blocking buffer) for 1 h at room temperature. Finally, membranes were scanned using the Odyssey (LICOR) imaging system.

Biotin-based internalization assay

Cells in 6 cm dishes were placed on ice and washed with cold PBS. Cell-surface receptors were labelled with 0.5 mg/ml cleavable biotin on ice for 30 min (EZlink cleavable sulfo-NHS-SS-biotin; Thermo Scientific, 21331) in Hanks' balanced salt solution (Sigma, H9269). Unbound biotin was washed away with cold PBS and internalization of receptors was triggered by addition of pre-warmed serum-free media and incubation at 37°C for the indicated time points with the exception of the 0 min time point. In this case, cold media was added to the 0 min dishes and cells were kept on ice to prevent internalization of receptors. For primaquine treatment, primaquine was diluted in PBS and added both to the biotin labelling mix and to the pre-warm mediums at a final concentration of 100 µM. Following internalization, for the indicated time points, cells were transferred to ice and surface biotin was cleaved away with 60 mM MesNa (Sigma, 63705) in MesNa buffer (50 mM Tris-HCl [pH 8.6], 100 mM NaCl) on ice for 30 min, followed by quenching with 100 mM iodoacetamide (IAA, Sigma, I1149-25G) on ice for 15 min. Cells were washed with cold PBS, scraped in 300 µl lysis buffer (50 mM Tris pH 7.5, 1.5 % Triton X-100, 100 mM NaCl, protease (Sigma, 4906837001) and phosphatase (Sigma, 5056489001) inhibitor tablets) and incubated at 4°C, with agitation, for 20 min. Afterward, the lysates were clarified by centrifugation (10,000xg, 10 min, 4°C), and

incubated overnight with a β1-integrin antibody, P5D2, for immunoprecipitation. Lysates were then incubated with protein G sepharose beads (GE Healthcare, 17-0618-01) for 2-3 h at 4°C and beads were washed 3 times with diluted lysis buffer (dilution of 1:3 in dH2O) followed by elution in non-reducing Laemmli sample buffer and denaturation for 5 min, 95°C. Western blotting was performed as described above and biotinylated (internalized) β1-integrin was detected by immunoblotting with horseradish peroxidase (HRP)-conjugated anti-biotin antibody (Cell Signaling Technology, 7075, 1:15000) and imaging with the chemiluminescence film-based system. Total β1-integrin was detected by immunoblotting the membrane again with clone N29 anti-β1-integrin antibody (Merck, MAB2252, 1:1000) and appropriate secondary antibody and analysis on the Odyssey (LICOR) imaging system. Biotin and total β1-integrin signals were quantified as integrated densities of protein bands with ImageJ (v. 1.43u), and the biotin signal was normalized to the corresponding total β1-integrin signal for each timepoint.

Co-Immunoprecipitation

Cells expressing GFP-conjugated proteins (one 10 cm dish per condition) were washed with cold PBS and detached with trypsin. Following centrifugation, 200 µl of IP-lysis buffer (40 mM Hepes-NaOH, 75 mM NaCl, 2 mM EDTA, 1% NP40, protease and phosphatase inhibitor tablets) was added to the cell pellet and cells were lysed at +4 °C for 30 min, followed by centrifugation (10,000xg for 10 min, +4 °C). 20 µl of the supernatant was kept aside as the lysis control. The remainder of the supernatant was incubated with GFP-Trap beads (ChromoTek; gtak-20) for 1 h at 4ºC. Finally, immunoprecipitated complexes were washed three times with wash-buffer (20 mM Tris-HCl (pH 7.5), 150 mM NaCl, 1 % NP-40) followed by denaturing for 5 min at 95ºC in reducing Laemmli buffer before analyses by SDS-PAGE followed by immunoblotting as above.

Subcellular fractionation

The protocol was modified from (Bass, Williamson et al. 2011b). Briefly, cells (one 10 cm dish) were washed with cold PBS and scraped off in 500 µl of hypotonic lysis buffer (10 mM HEPES-KOH pH 7.2, 0.25 M sucrose, 1 mM EDTA, 1 mM MgOAc and phosphatase and protease inhibitor tablets). Cells were lysed with the aid of a French press (approx. 30 passes) and 40 µl of total lysate was saved. The remaining lysate was then centrifuged at 1,000xg (10 min) to remove nuclei and cellular debris. The resulting supernatant was then centrifuged again at 10,000xg to collect the membrane fraction in pellet form and the cytosolic fraction as

supernatant. All fractionation steps were performed on ice. Finally, the reducing Laemmli buffer was added to fractions for 5 min at 95ºC before western blotting and immunoblotting as above.

Flow cytometry-based endocytosis assay

Attached cells were incubated with 1:500 diluted 12G10 or MAB13 antibodies in serum-free medium on ice for 30 min to allow the labelling of active and inactive cell-surface pools of β1-integrin, respectively. Unbound antibody was washed away in cold PBS and endocytosis was triggered by addition of pre-warmed serum-free medium to the cells and incubation at 37°C for 15 min and 30 min. In 0 min control cells, cold media was added and cells were kept on ice. Warm media was then removed and cells washed with cold PBS, detached with scraping the cells gently and fixed with 4 % PFA in PBS for 15 min at RT. Cells were then washed with PBS and incubated with the appropriate Alexa Fluor-conjugated secondary antibody (dilution 1:300 in PBS) for 1 h at 4°C. Cells were finally washed with PBS and analyzed with LSRFortessa (BD Biosciences). Data analysis was done using Flowing software version 2 (Cell Imaging Core of the Turku Centre for Biotechnology; www. http://flowingsoftware.btk.fi/).

Immunofluorescence, microscopy and image analysis.

Cells were plated either on 8-well slides (µ-Slide 8 well, ibiTreat; Ibidi, 80826) or on 3.5 mm dishes (Ibidi ibiTreat 35mm; Ibidi, 80136). Cells were fixed in 4 % paraformaldehyde for 15 min at room temperature, and following quenching of the fixative in 50 mM NH_4Cl for 15 min at room temperature, cells were permeabilized with 30 % horse serum in PBS containing 0.3 % Triton X-100 for 10 min at room temperature. Afterward, cells were incubated with primary antibodies (see key resources table) diluted in 30 % horse serum at +4°C, overnight. Later, cells were washed three times with PBS and appropriate secondary antibodies (see key resources table) diluted 1:250 in 30 % horse serum were added along with DAPI (1:5000) for 1 h at room temperature followed by three PBS washes. Samples were stored in PBS protected from light at 4°C until imaged and were imaged at room temperature. Middle plane images were acquired using a Carl Zeiss LSM880 laser scanning confocal microscope with Airyscan, a Carl Zeiss LSM780 laser scanning confocal or a 3i CSU-W1 spinning disk confocal microscope. For TIRF images wherever mentioned, bottom plane images were acquired using 63x objective of a Carl Zeiss TIRF microscope (Laser-TIRF 3 Imaging System). All the image analysis was done using FIJI (ImageJ version 1.49 k). Pearsons's correlation coefficient (R) of

colocalization was calculated using the coloc2 plugin in FIJI. Number of focal adhesions were calculated on paxillin channel by background subtraction (rolling ball radius=20) and applying median gaussian filter (3.0) followed by analysing the number of particles represented as focal adhesions and saving them as an image mask. For measuring the β1-integrin intensity in focal adhesions, focal adhesion mask from the paxillin channel was superimposed on 12G10 channel and mean intensity of 12G10 in each focal adhesion was measured.

ECM proteins and coating

Where indicated, wells were coated with 10 µg/mL collagen (PureCol® EZ Gel Bovine Collagen Solution, Type I; Advanced Biomatrix, 5074-G) or 10 µg/mL fibronectin (Merck-Millipore Calbiochem, 341631-5MG) in PBS for 1 h at 37°C. Unbound ligand (coating) was then removed, wells were blocked for 1 h at 37°C with 0.1% BSA and then washed with PBS before plating the cells in serum-free media.

Microscopy-based endocytosis assay

Cells were plated on 35 mm ibidi dishes, washed with PBS and incubated with 12G10 or MAB13 antibodies in Hanks' balanced salt solution on ice for 30 min to allow labelling of cell-surface active and inactive β1-integrin pools, respectively. Unbound antibody was washed away in cold PBS and endocytosis was triggered by addition of pre-warmed serum-free medium to the cells and incubation at 37°C for the indicated timepoints. In 0 min control cells, cold media was added and cells were kept on ice. The warm medium was then removed and cells washed with cold PBS, fixed, permeabilized, stained as described above and the middle plane of cells imaged with a Carl Zeiss LSM880 laser scanning confocal microscope with Airyscan (63x objective). For quantification of internalized integrin signal, the area of interest was drawn inside the cell excluding the plasma membrane and mean integrated density was measured using ImageJ.

Micropatterns and probabilistic density maps

Micropatterns were created on glass coverslips coated with fibronection as described in (Azioune, Storch et al. 2009). Cells in serum-free medium were seeded on micropatterns for 3 h before fixing and staining as described above.

Migration assay

Cells were plated on 24-well plates coated with 25 µg/ml fibronectin. Phase-contrast images were taken overnight, at 20 min intervals, using a Nikon Eclipse inverted widefield microscope (20x objective), equipped with a heated chamber (37°C) and CO_2 controller (5%). Cells were manually tracked using ImageJ and the resulting metafiles were imported into ibidi chemotaxis and Migration tool 2.0 to determine velocity and directionality and to create a visual representation of migration tracks. Dividing cells and cells making contacts were not considered for analysis.

Inverted invasion assay

200 µl of 5 µg/mL collagen (PureCol® EZ Gel Bovine Collagen Solution, Type I; Advanced Biomatrix, 5074-G) was placed into each transwell chamber (24 Well ThinCert™ Cell Culture Inserts; Greiner Bio-One, 662638) and incubated for 1 h at 37°C in a humidified incubator to set. Transwells were inverted on the lid of a 24-well plate and of 100,000 cells (100 µl volume) in complete medium were placed onto the underside of each transwell filter. Transwells were then covered with the 24-well plate touching the cell suspension drop. The inverted plate was incubated at 37°C for 2-4 h for the cells to attach. Later, transwells were removed, washed twice with serum-free media to remove serum and placed in new 24 well plates containing 1 ml of serum-free media. 100 µl of medium containing 10% FBS as a chemoattractant was pipetted on top of the collagen plug and incubated for 3 days. For visualization, transwells were transferred to a fresh 24-well plate, fixed with 4% PFA for 2 h and stained for actin (phalloidin) after permeabilization with 0.3 % (vol/vol) Triton-X 100 for 30 min at room temperature. Virtual 3D Imaging was done with Zeiss LSM510 confocal microscope using 20x objective. Individual confocal images were represented in sequence with increasing penetrance of cells from left to right. The invasion was quantified using the area calculator plugin of ImageJ, measuring the fluorescence intensity of cells invading 60 µm or more and expressing this as a percentage of the fluorescence intensity of all cells within the plug.

In vitro 2D Proliferation assay

Control siRNA or GGA2 siRNA silenced cells were plated on 96-well plates (100 µl; 3000 cells/well). After 1 d, 2 d and 4 d of cell growth, of WST-8 reagent (cell counting kit 8, Sigma-Aldrich,96992) was added to each well (10 µl/well) and absorbance was measured at 450 nm by a plate reader (Thermo, Multiskan Ascent 96/384) after 1 h incubation at +37ºC. Culture

medium without cells was used to measure background. Relative proliferation was calculated by normalizing the A450 values of 2 d and 4 d to 1 d after background subtraction.

Mammosphere formation assay

Cells (1000 cells per condition) were plated on 96-well low attachment plates (Corning® Costar® Ultra-Low attachment multiwell plates; Corning, CLS3474-24EA) in Epicult Base medium (StemCell Technologies) supplemented with Epicult supplements, 10 ng/ml EGF, 4 µg/ml heparin and 10 ng/ml bFGF. Cells were allowed to proliferate for 7 days. Mammospheres were counted manually and images captured using the EVOS® Cell Imaging System (ThermoFisher Scientific).

BioID proximity biotinylation pulldown assay

The protocol was modified from (Roux, Kim et al. 2013) for MDA-MB-231 cells and the BioID-GGA2 construct. Briefly, three 10 cm dishes were transiently transfected per condition (Myc-BioID construct, Myc-BioID-GGA2 construct or mock transfection) in Opti-MEM™ (ThermoFisher, 31985070) containing 50 µM Biotin (Sigma, B4501). After 18 h, media was removed and cells were washed with cold PBS and lysed in 500 µl lysis buffer (0.1% SDS, 0.1% Deoxycholate, 1% TritonX-100, 1mM EDTA, 200mM NaCl, 50 mM HEPES pH 7.5, protease and phosphatase inhibitor tablets) for each dish. The lysates were passed through a 27G needle 10 times and incubated for 20 min at 4°C with agitation. Cell lysates were cleared by centrifuge at 10,000xg, 10 min at 4°C and supernatants from the same condition were pooled and added to fresh 2 ml tubes containing magnetic streptavidin beads (Dynabeads® MyOne™ Streptavidin C1; Life Technologies, 65001) pre-washed with 1:3 lysis buffer and incubated overnight at 4°C with agitation. On the following day, supernatants were removed from the tubes and beads were washed once in buffer1 (0.5% deoxycholate, 0.5% NP-40, 1 mM EDTA, 250 mM LiCl, 10 mM Tris-Cl pH 7.4, protease and phosphatase inhibitor tablets) for 5 min and then in buffer2 (200 mM NaCl, 75 mM Tris-Cl pH 7.4, 7.5 mM EDTA, 7.5 mM EGTA, 1.5% TritonX-100, 0.75% NP-40, protease and phosphatase inhibitor tablets) for 5 min. Finally, proteins were eluted from the beads in 50 µl of reducing SDS sample buffer for 5 min at 95°C and separated by SDS-PAGE. The gel was then stained with Coomassie blue and each lane was cut carefully into 5-8 pieces for in gel-digestion and mass spectrometry analysis.

Mass spectrometry analysis

Proteins cut from an SDS-PAGE gel were in-gel digested by trypsin according to a standard protocol (Shevchenko, Wilm et al. 1996). The LC-ESI-MS/MS analyses were performed on a nanoflow HPLC system (Easy-nLCII, Thermo Fisher Scientific) coupled to the LTQ Orbitrap Velos Pro mass spectrometer (Thermo Fisher Scientific, Bremen, Germany) equipped with a nano-electrospray ionization source. Peptides were first loaded on a trapping column and subsequently separated inline on a 15 cm C18 column (75 µm x 15 cm, ReproSil-Pur 5 µm 200 Å C18-AQ, Dr. Maisch HPLC GmbH, Ammerbuch-Entringen, Germany). The mobile phase consisted of water/acetonitrile (98:2 (v/v)) with 0.1% formic acid (solvent A) and acetonitrile/water (95:5 (v/v)) with 0.1% formic acid (solvent B). A two-step 45 min gradient from 5% to 40% B was used to elute peptides.

MS data were acquired automatically by using Thermo Xcalibur 3.0 software (Thermo Fisher Scientific). An information dependent acquisition method consisted of an Orbitrap MS survey scan of mass range 300-2000 m/z followed by CID fragmentation for 10 most intense peptide ions. Fragmentation, and detection of fragment ions (MS2 scan), was performed in a linear ion trap.

The data files were searched for protein identification using Proteome Discoverer 1.4 software (Thermo Fisher Scientific) connected to an in-house Mascot server running the Mascot 2.5 software (Matrix Science). Data were searched against the SwissProt database (release 2015_08). The search included carbamidomethyl as a fixed modification and methionine oxidation as variable modification together with one tryptic missed cleavage. The peptide and protein false discovery rate (FDR) was set to 5%. Proteins assigned at least with two peptides were accepted.

Antibodies and siRNAs

These are indicated in the table below

Antibodies	Species	Source	Catalog number	Application
Total β1-integrin, clone N29	mouse	Merck-Millipore	MAB2252	WB
Total β1-integrin, clone P5D2	mouse	Developmental Studies Hybridoma Bank		IF
Active β1-integrin, clone 9EG7	rat	BD Biosciences	55371	IF
Active β1-integrin, clone 12G10	mouse	Developmental Studies Hybridoma Bank		IF
				FACS
Inactive β1-integrin, clone MAB13	rat	Developmental Studies Hybridoma Bank		IF
				FACS
Biotin-HRP	goat	Cell Signaling Technologies	#7075	WB
Transferrin Receptor (TfR)	rabbit	Abcam	ab84036	WB
alpha-tubulin	mouse	Hybridoma bank		WB
GGA2	mouse	BD Biosciences	612612	WB
				IF
GFP	rabbit	Abcam	ab290	WB
RAB5	rabbit	Cell Signaling Technologies	3547S	IF
RAB4	rabbit	Cell Signaling Technologies	2167S	IF
RAB11	rabbit	Cell Signaling Technologies	5589S	IF
EEA1	rabbit	Cell Signaling Technologies	3288S	IF
VPS35	goat	Abcam	ab10099	IF
RAB7	rabbit	Cell Signaling Technologies	9367S	IF
LAMP1, clone H4A3	mouse	Santa Cruz Biotechnology	SC-20011	IF
CLTC	rabbit	Abcam	ab21679	IF WB
TGN46	rabbit	Abcam	ab50595	IF
RAB6	rabbit	Cell Signaling Technologies	9625S	IF
Na-k pump, clone a6F	mouse	Developmental Studies Hybridoma Bank		WB

paxillin	rabbit	Santa Cruz Biotechnology	sc-5574	IF
RAB13	rabbit	Novus	NBP1-85799	WB
				IF
RAB10, clone 4E2	mouse	Millipore	MABN730	WB
c-Myc tag	mouse	Covance	MMS-150R-1000	WB
				IF
streptavidin-Alexa 488	none	Invitrogen	S11223	IF
GGA1	rabbit	Invitrogen	PA5-61699	WB
GGA3	mouse	BD Biosciences	612310	WB
anti-mouse IRDye 800CW	donkey	LI-COR Biosciences	926-32212	WB
anti-mouse IRDye 680RD	donkey	LI-COR Biosciences	926-68072	WB
anti-rabbit IRDye 800CW	donkey	LI-COR Biosciences	926-32213)	WB
anti-rabbit IRDye 680RD	donkey	LI-COR Biosciences	926-68073	WB
siRNA	**Target gene**	**Source**	**Identifier**	
siCTRL	none	Qiagen	SI03650318	
siGGA2#1	*GGA2*	Qiagen	SI03190012	
siGGA2#2	*GGA2*	Integrated DNA Technologies IDT	hs.Ri.GGA2.13.1	
siRAB13#1	*RAB13*	Integrated DNA Technologies IDT	hs.Ri.RAB13.13.1	
siRAB13#2	*RAB13*	Integrated DNA Technologies IDT	hs.Ri.RAB13.13.1	
siRAB10#1	*RAB10*	Integrated DNA Technologies IDT	hs.Ri.RAB10.13.1	

References

ALANKO, J., MAI, A., JACQUEMET, G., SCHAUER, K., KAUKONEN, R., SAARI, M., GOUD, B. and IVASKA, J., 2015. Integrin endosomal signalling suppresses anoikis. *Nature cell biology,* **17**(11), pp. 1412-1421.

ARGENZIO, E., MARGADANT, C., LEYTON-PUIG, D., JANSSEN, H., JALINK, K., SONNENBERG, A. and MOOLENAAR, W.H., 2014. CLIC4 regulates cell adhesion and beta1 integrin trafficking. *Journal of cell science,* **127**(Pt 24), pp. 5189-5203.

ARJONEN, A., ALANKO, J., VELTEL, S. and IVASKA, J., 2012. Distinct recycling of active and inactive beta1 integrins. *Traffic (Copenhagen, Denmark),* **13**(4), pp. 610-625.

AZIOUNE, A., STORCH, M., BORNENS, M., THERY, M. and PIEL, M., 2009. Simple and rapid process for single cell micro-patterning. *Lab on a chip,* **9**(11), pp. 1640-1642.

BASS, M.D., WILLIAMSON, R.C., NUNAN, R.D., HUMPHRIES, J.D., BYRON, A., MORGAN, M.R., MARTIN, P. and HUMPHRIES, M.J., 2011a. A syndecan-4 hair trigger initiates wound healing through caveolin- and RhoG-regulated integrin endocytosis. *Developmental cell,* **21**(4), pp. 681-693.

BASS, M.D., WILLIAMSON, R.C., NUNAN, R.D., HUMPHRIES, J.D., BYRON, A., MORGAN, M.R., MARTIN, P. and HUMPHRIES, M.J., 2011b. A syndecan-4 hair trigger initiates wound healing through caveolin- and RhoG-regulated integrin endocytosis. *Developmental cell,* **21**(4), pp. 681-693.

BOMAN, A.L., ZHANG, C., ZHU, X. and KAHN, R.A., 2000. A family of ADP-ribosylation factor effectors that can alter membrane transport through the trans-Golgi. *Molecular biology of the cell,* **11**(4), pp. 1241-1255.

BOTTCHER, R.T., STREMMEL, C., MEVES, A., MEYER, H., WIDMAIER, M., TSENG, H.Y. and FASSLER, R., 2012. Sorting nexin 17 prevents lysosomal degradation of beta1 integrins by binding to the beta1-integrin tail. *Nature cell biology,* **14**(6), pp. 584-592.

BRIDGEWATER, R.E., NORMAN, J.C. and CASWELL, P.T., 2012. Integrin trafficking at a glance. *Journal of cell science,* **125**(Pt 16), pp. 3695-3701.

CALDERWOOD, D.A., CAMPBELL, I.D. and CRITCHLEY, D.R., 2013a. Talins and kindlins: partners in integrin-mediated adhesion. *Nature reviews.Molecular cell biology,* **14**(8), pp. 503-517.

CALDERWOOD, D.A., CAMPBELL, I.D. and CRITCHLEY, D.R., 2013b. Talins and kindlins: partners in integrin-mediated adhesion. *Nature reviews.Molecular cell biology,* **14**(8), pp. 503-517.

CAMPBELL, I.D. and HUMPHRIES, M.J., 2011. Integrin structure, activation, and interactions. *Cold Spring Harbor perspectives in biology,* **3**(3), pp. 10.1101/cshperspect.a004994.

CASWELL, P.T., CHAN, M., LINDSAY, A.J., MCCAFFREY, M.W., BOETTIGER, D. and NORMAN, J.C., 2008. Rab-coupling protein coordinates recycling of alpha5beta1 integrin and EGFR1 to promote cell migration in 3D microenvironments. *The Journal of cell biology,* **183**(1), pp. 143-155.

CASWELL, P.T., SPENCE, H.J., PARSONS, M., WHITE, D.P., CLARK, K., CHENG, K.W., MILLS, G.B., HUMPHRIES, M.J., MESSENT, A.J., ANDERSON, K.I., MCCAFFREY, M.W., OZANNE, B.W. and NORMAN, J.C., 2007. Rab25 associates with alpha5beta1 integrin to promote invasive migration in 3D microenvironments. *Developmental cell,* **13**(4), pp. 496-510.

DE FRANCESCHI, N., HAMIDI, H., ALANKO, J., SAHGAL, P. and IVASKA, J., 2015. Integrin traffic - the update. *Journal of cell science,* **128**(5), pp. 839-852.

DELL'ANGELICA, E.C., PUERTOLLANO, R., MULLINS, C., AGUILAR, R.C., VARGAS, J.D., HARTNELL, L.M. and BONIFACINO, J.S., 2000. GGAs: a family of ADP ribosylation factor-binding proteins related to adaptors and associated with the Golgi complex. *The Journal of cell biology,* **149**(1), pp. 81-94.

DIGGINS, N.L., KANG, H., WEAVER, A. and WEBB, D.J., 2018. alpha5beta1 integrin trafficking and Rac activation are regulated by APPL1 in a Rab5-dependent manner to inhibit cell migration. *Journal of cell science,* **131**(5), pp. 10.1242/jcs.207019.

DOZYNKIEWICZ, M.A., JAMIESON, N.B., MACPHERSON, I., GRINDLAY, J., VAN DEN BERGHE, P.V., VON THUN, A., MORTON, J.P., GOURLEY, C., TIMPSON, P., NIXON, C., MCKAY, C.J., CARTER, R., STRACHAN, D., ANDERSON, K., SANSOM, O.J., CASWELL, P.T. and NORMAN, J.C., 2012. Rab25 and CLIC3 collaborate to promote integrin recycling from late endosomes/lysosomes and drive cancer progression. *Developmental cell,* **22**(1), pp. 131-145.

FELDING-HABERMANN, B., O'TOOLE, T.E., SMITH, J.W., FRANSVEA, E., RUGGERI, Z.M., GINSBERG, M.H., HUGHES, P.E., PAMPORI, N., SHATTIL, S.J., SAVEN, A. and MUELLER, B.M., 2001. Integrin activation controls metastasis in human breast cancer. *Proceedings of the National Academy of Sciences of the United States of America,* **98**(4), pp. 1853-1858.

FLETCHER, S.J. and RAPPOPORT, J.Z., 2010. Moving forward: polarised trafficking in cell migration. *Trends in cell biology,* **20**(2), pp. 71-78.

GHOSH, P., GRIFFITH, J., GEUZE, H.J. and KORNFELD, S., 2003. Mammalian GGAs act together to sort mannose 6-phosphate receptors. *The Journal of cell biology,* **163**(4), pp. 755-766.

GOVERO, J., DORAY, B., BAI, H. and KORNFELD, S., 2012. Analysis of Gga null mice demonstrates a non-redundant role for mammalian GGA2 during development. *PloS one,* **7**(1), pp. e30184.

GU, Z., NOSS, E.H., HSU, V.W. and BRENNER, M.B., 2011. Integrins traffic rapidly via circular dorsal ruffles and macropinocytosis during stimulated cell migration. *The Journal of cell biology,* **193**(1), pp. 61-70.

HEGDE, S. and RAGHAVAN, S., 2013. A skin-depth analysis of integrins: role of the integrin network in health and disease. *Cell communication & adhesion,* **20**(6), pp. 155-169.

HIRST, J., BORNER, G.H., ANTROBUS, R., PEDEN, A.A., HODSON, N.A., SAHLENDER, D.A. and ROBINSON, M.S., 2012. Distinct and overlapping roles for AP-1 and GGAs revealed by the "knocksideways" system. *Current biology : CB,* **22**(18), pp. 1711-1716.

HIRST, J., LUI, W.W., BRIGHT, N.A., TOTTY, N., SEAMAN, M.N. and ROBINSON, M.S., 2000. A family of proteins with gamma-adaptin and VHS domains that facilitate trafficking between the trans-Golgi network and the vacuole/lysosome. *The Journal of cell biology,* **149**(1), pp. 67-80.

HUANG, R. and ROFSTAD, E.K., 2018. Integrins as therapeutic targets in the organ-specific metastasis of human malignant melanoma. *Journal of experimental & clinical cancer research : CR,* **37**(1), pp. 92-018-0763-x.

HUTAGALUNG, A.H. and NOVICK, P.J., 2011. Role of Rab GTPases in membrane traffic and cell physiology. *Physiological Reviews,* **91**(1), pp. 119-149.

HYNES, R.O., 2002. Integrins: bidirectional, allosteric signaling machines. *Cell,* **110**(6), pp. 673-687.

IOANNOU, M.S., BELL, E.S., GIRARD, M., CHAINEAU, M., HAMLIN, J.N., DAUBARAS, M., MONAST, A., PARK, M., HODGSON, L. and MCPHERSON, P.S., 2015. DENND2B activates Rab13 at the leading edge of migrating cells and promotes metastatic behavior. *The Journal of cell biology,* **208**(5), pp. 629-648.

JEAN, C., GRAVELLE, P., FOURNIE, J.J. and LAURENT, G., 2011. Influence of stress on extracellular matrix and integrin biology. *Oncogene,* **30**(24), pp. 2697-2706.

JIN, J.K., TIEN, P.C., CHENG, C.J., SONG, J.H., HUANG, C., LIN, S.H. and GALLICK, G.E., 2015. Talin1 phosphorylation activates beta1 integrins: a novel mechanism to promote prostate cancer bone metastasis. *Oncogene,* **34**(14), pp. 1811-1821.

JONKER, C.T.H., GALMES, R., VEENENDAAL, T., TEN BRINK, C., VAN DER WELLE, R.E.N., LIV, N., DE ROOIJ, J., PEDEN, A.A., VAN DER SLUIJS, P., MARGADANT, C. and KLUMPERMAN, J., 2018. Vps3 and Vps8 control integrin trafficking from early to recycling endosomes and regulate integrin-dependent functions. *Nature communications,* **9**(1), pp. 792-018-03226-8.

KAWAUCHI, T., 2012. Cell adhesion and its endocytic regulation in cell migration during neural development and cancer metastasis. *International journal of molecular sciences,* **13**(4), pp. 4564-4590.

LIU, J., DAS, M., YANG, J., ITHYCHANDA, S.S., YAKUBENKO, V.P., PLOW, E.F. and QIN, J., 2015. Structural mechanism of integrin inactivation by filamin. *Nature structural & molecular biology,* **22**(5), pp. 383-389.

MAI, A., VELTEL, S., PELLINEN, T., PADZIK, A., COFFEY, E., MARJOMAKI, V. and IVASKA, J., 2011. Competitive binding of Rab21 and p120RasGAP to integrins regulates receptor traffic and migration. *The Journal of cell biology,* **194**(2), pp. 291-306.

MCNALLY, K.E., FAULKNER, R., STEINBERG, F., GALLON, M., GHAI, R., PIM, D., LANGTON, P., PEARSON, N., DANSON, C.M., NAGELE, H., MORRIS, L.L., SINGLA, A., OVERLEE, B.L., HEESOM, K.J., SESSIONS, R., BANKS, L., COLLINS, B.M., BERGER, I., BILLADEAU, D.D., BURSTEIN, E. and CULLEN, P.J., 2017. Retriever is a multiprotein complex for retromer-independent endosomal cargo recycling. *Nature cell biology,* **19**(10), pp. 1214-1225.

NADER, G.P., EZRATTY, E.J. and GUNDERSEN, G.G., 2016. FAK, talin and PIPKIgamma regulate endocytosed integrin activation to polarize focal adhesion assembly. *Nature cell biology,* **18**(5), pp. 491-503.

NIELSEN, M.S., MADSEN, P., CHRISTENSEN, E.I., NYKJAER, A., GLIEMANN, J., KASPER, D., POHLMANN, R. and PETERSEN, C.M., 2001. The sortilin cytoplasmic tail conveys Golgi-endosome transport and binds the VHS domain of the GGA2 sorting protein. *The EMBO journal,* **20**(9), pp. 2180-2190.

NISHIKIMI, A., ISHIHARA, S., OZAWA, M., ETOH, K., FUKUDA, M., KINASHI, T. and KATAGIRI, K., 2014. Rab13 acts downstream of the kinase Mst1 to deliver the integrin LFA-1 to the cell surface for lymphocyte trafficking. *Science signaling,* **7**(336), pp. ra72.

NOKES, R.L., FIELDS, I.C., COLLINS, R.N. and FOLSCH, H., 2008a. Rab13 regulates membrane trafficking between TGN and recycling endosomes in polarized epithelial cells. *The Journal of cell biology,* **182**(5), pp. 845-853.

NOKES, R.L., FIELDS, I.C., COLLINS, R.N. and FOLSCH, H., 2008b. Rab13 regulates membrane trafficking between TGN and recycling endosomes in polarized epithelial cells. *The Journal of cell biology,* **182**(5), pp. 845-853.

PARACHONIAK, C.A., LUO, Y., ABELLA, J.V., KEEN, J.H. and PARK, M., 2011. GGA3 functions as a switch to promote Met receptor recycling, essential for sustained ERK and cell migration. *Developmental cell,* **20**(6), pp. 751-763.

PARACHONIAK, C.A. and PARK, M., 2012. Dynamics of receptor trafficking in tumorigenicity. *Trends in cell biology,* **22**(5), pp. 231-240.

PAUL, N.R., ALLEN, J.L., CHAPMAN, A., MORLAN-MAIRAL, M., ZINDY, E., JACQUEMET, G., FERNANDEZ DEL AMA, L., FERIZOVIC, N., GREEN, D.M., HOWE, J.D., EHLER, E., HURLSTONE, A. and CASWELL, P.T., 2015. alpha5beta1 integrin recycling promotes Arp2/3-independent cancer cell invasion via the formin FHOD3. *The Journal of cell biology,* **210**(6), pp. 1013-1031.

PAUL, N.R., JACQUEMET, G. and CASWELL, P.T., 2015. Endocytic Trafficking of Integrins in Cell Migration. *Current biology : CB,* **25**(22), pp. R1092-105.

PEKKONEN, P., ALVE, S., BALISTRERI, G., GRAMOLELLI, S., TATTI-BUGAEVA, O., PAATERO, I., NIIRANEN, O., TUOHINTO, K., PERALA, N., TAIWO, A., ZINOVKINA,

N., REPO, P., ICAY, K., IVASKA, J., SAHARINEN, P., HAUTANIEMI, S., LEHTI, K. and OJALA, P.M., 2018. Lymphatic endothelium stimulates melanoma metastasis and invasion via MMP14-dependent Notch3 and beta1-integrin activation. *eLife,* **7**, pp. 10.7554/eLife.32490.

PELLINEN, T., ARJONEN, A., VUORILUOTO, K., KALLIO, K., FRANSEN, J.A. and IVASKA, J., 2006. Small GTPase Rab21 regulates cell adhesion and controls endosomal traffic of beta1-integrins. *The Journal of cell biology,* **173**(5), pp. 767-780.

POWELKA, A.M., SUN, J., LI, J., GAO, M., SHAW, L.M., SONNENBERG, A. and HSU, V.W., 2004a. Stimulation-dependent recycling of integrin beta1 regulated by ARF6 and Rab11. *Traffic (Copenhagen, Denmark),* **5**(1), pp. 20-36.

POWELKA, A.M., SUN, J., LI, J., GAO, M., SHAW, L.M., SONNENBERG, A. and HSU, V.W., 2004b. Stimulation-dependent recycling of integrin beta1 regulated by ARF6 and Rab11. *Traffic (Copenhagen, Denmark),* **5**(1), pp. 20-36.

POZZI, A. and ZENT, R., 2013. Integrins in kidney disease. *Journal of the American Society of Nephrology : JASN,* **24**(7), pp. 1034-1039.

PUERTOLLANO, R. and BONIFACINO, J.S., 2004. Interactions of GGA3 with the ubiquitin sorting machinery. *Nature cell biology,* **6**(3), pp. 244-251.

PUERTOLLANO, R., RANDAZZO, P.A., PRESLEY, J.F., HARTNELL, L.M. and BONIFACINO, J.S., 2001. The GGAs promote ARF-dependent recruitment of clathrin to the TGN. *Cell,* **105**(1), pp. 93-102.

RAINERO, E. and NORMAN, J.C., 2015. Endosomal integrin signals for survival. *Nature cell biology,* **17**(11), pp. 1373-1375.

RANTALA, J.K., MAKELA, R., AALTOLA, A.R., LAASOLA, P., MPINDI, J.P., NEES, M., SAVIRANTA, P. and KALLIONIEMI, O., 2011. A cell spot microarray method for production of high density siRNA transfection microarrays. *BMC genomics,* **12**, pp. 162-2164-12-162.

RANTALA, J.K., POUWELS, J., PELLINEN, T., VELTEL, S., LAASOLA, P., MATTILA, E., POTTER, C.S., DUFFY, T., SUNDBERG, J.P., KALLIONIEMI, O., ASKARI, J.A., HUMPHRIES, M.J., PARSONS, M., SALMI, M. and IVASKA, J., 2011. SHARPIN is an endogenous inhibitor of beta1-integrin activation. *Nature cell biology,* **13**(11), pp. 1315-1324.

RATCLIFFE, C.D., SAHGAL, P., PARACHONIAK, C.A., IVASKA, J. and PARK, M., 2016. Regulation of Cell Migration and beta1 Integrin Trafficking by the Endosomal Adaptor GGA3. *Traffic (Copenhagen, Denmark),* **17**(6), pp. 670-688.

ROUX, K.J., KIM, D.I. and BURKE, B., 2013. BioID: a screen for protein-protein interactions. *Current protocols in protein science,* **74**, pp. Unit 19.23.

ROUX, K.J., KIM, D.I., RAIDA, M. and BURKE, B., 2012. A promiscuous biotin ligase fusion protein identifies proximal and interacting proteins in mammalian cells. *The Journal of cell biology,* **196**(6), pp. 801-810.

SCHINDELIN, J., ARGANDA-CARRERAS, I., FRISE, E., KAYNIG, V., LONGAIR, M., PIETZSCH, T., PREIBISCH, S., RUEDEN, C., SAALFELD, S., SCHMID, B., TINEVEZ, J.Y., WHITE, D.J., HARTENSTEIN, V., ELICEIRI, K., TOMANCAK, P. and CARDONA, A., 2012. Fiji: an open-source platform for biological-image analysis. *Nature methods,* **9**(7), pp. 676-682.

SCOTT, P.M., BILODEAU, P.S., ZHDANKINA, O., WINISTORFER, S.C., HAUGLUND, M.J., ALLAMAN, M.M., KEARNEY, W.R., ROBERTSON, A.D., BOMAN, A.L. and PIPER, R.C., 2004. GGA proteins bind ubiquitin to facilitate sorting at the trans-Golgi network. *Nature cell biology,* **6**(3), pp. 252-259.

SHEVCHENKO, A., WILM, M., VORM, O. and MANN, M., 1996. Mass spectrometric sequencing of proteins silver-stained polyacrylamide gels. *Analytical Chemistry,* **68**(5), pp. 850-858.

SHIBA, Y., KATOH, Y., SHIBA, T., YOSHINO, K., TAKATSU, H., KOBAYASHI, H., SHIN, H.W., WAKATSUKI, S. and NAKAYAMA, K., 2004. GAT (GGA and Tom1) domain responsible for ubiquitin binding and ubiquitination. *The Journal of biological chemistry,* **279**(8), pp. 7105-7111.

STEINBERG, F., HEESOM, K.J., BASS, M.D. and CULLEN, P.J., 2012. SNX17 protects integrins from degradation by sorting between lysosomal and recycling pathways. *The Journal of cell biology,* **197**(2), pp. 219-230.

STENMARK, H., 2009. Rab GTPases as coordinators of vesicle traffic. *Nature reviews.Molecular cell biology,* **10**(8), pp. 513-525.

SUBRAMANI, D. and ALAHARI, S.K., 2010. Integrin-mediated function of Rab GTPases in cancer progression. *Molecular cancer,* **9**, pp. 312-4598-9-312.

TAKATSU, H., KATOH, Y., SHIBA, Y. and NAKAYAMA, K., 2001. Golgi-localizing, gamma-adaptin ear homology domain, ADP-ribosylation factor-binding (GGA) proteins interact with acidic dileucine sequences within the cytoplasmic domains of sorting receptors through their Vps27p/Hrs/STAM (VHS) domains. *The Journal of biological chemistry,* **276**(30), pp. 28541-28545.

THERY, M., 2010. Micropatterning as a tool to decipher cell morphogenesis and functions. *Journal of cell science,* **123**(Pt 24), pp. 4201-4213.

UEMURA, T., KAMETAKA, S. and WAGURI, S., 2018. GGA2 interacts with EGFR cytoplasmic domain to stabilize the receptor expression and promote cell growth. *Scientific reports,* **8**(1), pp. 1368-018-19542-4.

WANG, S., HU, C., WU, F. and HE, S., 2017. Rab25 GTPase: Functional roles in cancer. *Oncotarget,* **8**(38), pp. 64591-64599.

WHITE, R.M., SESSA, A., BURKE, C., BOWMAN, T., LEBLANC, J., CEOL, C., BOURQUE, C., DOVEY, M., GOESSLING, W., BURNS, C.E. and ZON, L.I., 2008. Transparent adult zebrafish as a tool for in vivo transplantation analysis. *Cell stem cell,* **2**(2), pp. 183-189.

WINOGRAD-KATZ, S.E., FASSLER, R., GEIGER, B. and LEGATE, K.R., 2014. The integrin adhesome: from genes and proteins to human disease. *Nature reviews.Molecular cell biology,* **15**(4), pp. 273-288.

YE, F., SNIDER, A.K. and GINSBERG, M.H., 2014. Talin and kindlin: the one-two punch in integrin activation. *Frontiers of medicine,* **8**(1), pp. 6-16.

ZHAO, Y. and KEEN, J.H., 2008a. Gyrating clathrin: highly dynamic clathrin structures involved in rapid receptor recycling. *Traffic (Copenhagen, Denmark),* **9**(12), pp. 2253-2264.

ZHAO, Y. and KEEN, J.H., 2008b. Gyrating clathrin: highly dynamic clathrin structures involved in rapid receptor recycling. *Traffic (Copenhagen, Denmark),* **9**(12), pp. 2253-2264.

ZHU, Y., DORAY, B., POUSSU, A., LEHTO, V.P. and KORNFELD, S., 2001a. Binding of GGA2 to the lysosomal enzyme sorting motif of the mannose 6-phosphate receptor. *Science (New York, N.Y.),* **292**(5522), pp. 1716-1718.

ZHU, Y., DORAY, B., POUSSU, A., LEHTO, V.P. and KORNFELD, S., 2001b. Binding of GGA2 to the lysosomal enzyme sorting motif of the mannose 6-phosphate receptor. *Science (New York, N.Y.),* **292**(5522), pp. 1716-1718.